

Contents

1	Theoretical Background	1
1.1	Plasma	1
1.1.1	Plasma Parameters	2
1.2	Single Particle Motion	5
1.2.1	Gyration	5
1.2.2	E-cross-B Drift	6
1.3	Kinetic Theory	8
1.4	Fluid Description	8
1.4.1	Velocity Moments	8
1.4.2	Transport Equation	9
1.4.3	Fluid Equations	10
1.4.4	Plasma States	10
1.5	Plasma Oscillations	11
1.6	Magnetohydrodynamics	13
1.7	Numerical Simulations	13
2	Method	15
2.1	Particle-in-Cell	15
2.1.1	Movers	16
2.1.2	Field Solvers	17
2.2	Stability	18
2.2.1	Time Stability Criterion	18
2.2.2	Spatial Stability Criterion	19
2.2.3	Finite Grid Instability	20
2.3	Normalization	20
2.3.1	Non-dimensionality PinC	20
2.3.2	Normalization PinC	22
2.3.3	Mover	22
2.3.4	Accelerator	23
2.3.5	Distribute	23
2.3.6	Solver	23
2.4	Grid Structs and Partitioning	24

Contents

2.4.1	Data structures	24
2.4.2	Domain partitioning	24
2.4.3	Singular domain	24
2.4.4	Several subdomains	25
2.5	Multigrid - Expanded	25
2.5.1	Algorithm	27
2.5.2	Smoothing	29
2.5.3	Restriction	31
2.5.4	Prolongation	32
2.6	Boundary conditions	32
2.6.1	Periodic Boundaries	34
2.6.2	Dirichlet Boundaries	34
2.6.3	Neumann Boundaries	34
2.6.4	Boundaries in Multigrid	35
2.6.5	Mixed Conditions	36
2.7	Parallelization	36
2.7.1	Grid Partition	36
2.7.2	Distributed and accumulated data	38
2.7.3	Smoothing	39
2.7.4	Restriction	39
2.7.5	Interpolation	39
2.7.6	Scaling	40
3	Implementation	43
3.1	General idea	43
3.1.1	V-cycle	43
3.1.2	Updating the Halo	44
3.1.3	Implementation	46
3.2	Restriction	46
3.3	Prolongation	47
3.4	Smoothers	49
3.5	Implementation of Boundary Conditions	51
3.5.1	Restriction	51
3.5.2	Periodic	51
3.5.3	Dirichlet	51
3.5.4	Neumann	51
4	Implementation	53
4.1	General idea	53
4.1.1	V-cycle	53
4.1.2	Updating the Halo	54
4.1.3	Implementation	56
4.2	Restriction	56

Contents

4.3	Prolongation	57
4.4	Smoothers	59
4.5	Implementation of Boundary Conditions	61
4.5.1	Restriction	61
4.5.2	Periodic	61
4.5.3	Dirichlet	61
4.5.4	Neumann	61
5	Verification	63
5.0.1	Error Quantification	63
5.1	Multigrid Solver	63
5.1.1	Analytical Solutions	64
5.1.2	Random Charge distribution	65
5.2	Scaling of the error compared to discretization	65
5.2.1	Langmuir Oscillation Test Case	67
5.3	Plasma Oscillation	67
5.3.1	Input parameters	68
6	Performance/Results	69
6.1	Scaling	69
6.1.1	Perfomance Optimizer	69
6.2	Processor scaling	70
6.2.1	Convergence Rate	70
6.2.2	Scaling of the MG Solver	70
6.2.3	Scaling properties PiC	71

Chapter 1

Theoretical Background

1.1 Plasma

This section presents a short overview of basic plasma theory, it can serve as a quick reminder for those already familiar with the subject, and necessary background to understand the numerical simulations in this work. For a more thorough introduction the books *Plasma Physics* (Fitzpatrick, 2014), *Introduction to Plasma Physics* (Goldston and Rutherford, 1995), *Waves and Oscillations in Plasmas* (Pécseli, 2012) or the classic *Introduction to Plasma Physics and Controlled Fusion* (Chen, 1984) can be consulted.

Plasma is the fourth, lesser known, state of matter. It is similar to a gas in that the particles are free to move, but it has the key distinction that a part of its constituent particles are electrically charged.

”A plasma is a quasineutral gas of charged and neutral particles which exhibits collective behaviour.”

Francis F. Chen

The charge causes the particles to be subject to the Lorentz force, which changes the behaviour of the gas. The plasma state is a typical state of matter and appears in various environments, i.e. the sun, and other stars, the upper parts of Earth’s atmosphere, and has many industrial applications as plasma cutters , argon light tubes, fusion.

A greater understanding of the mechanism governing a plasma’s behaviour can help us predict spaceweather, improve design of spacecraft and instruments affected by plasma.

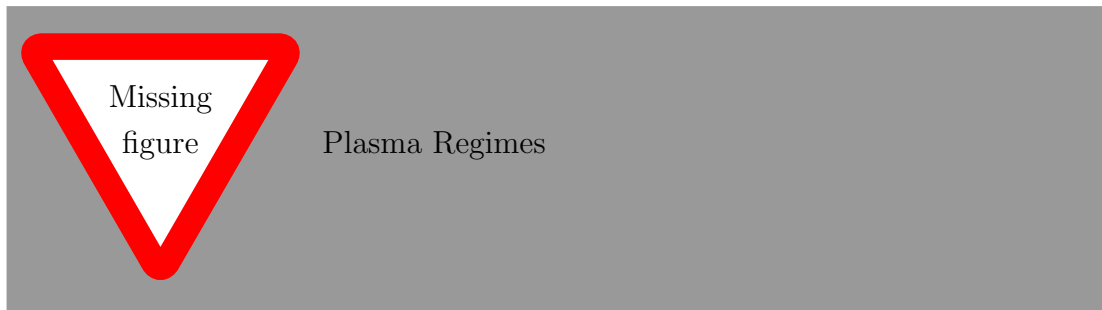


Figure 1.1: Plasmas occurs both in the hot and dense condiotions in necessary for fusion, as well as in the cold and sparse interstellar environment.

1.1.1 Plasma Parameters

Temperature

A modern view of temperature comes from kinetic theory developed by Maxwell and Boltzmann (Swendsen, 2006). We will not go through it here but a treatment is available in Goldston and Rutherford (1995). Temperature is then related to the average kinetic energy of a particle. For an ideal monoatomic gas the kinetic energy is then

$$\bar{E}_k = \frac{1}{2}mv_{th}^2 = \frac{3}{2}kT \quad (1.1)$$

Here we have introduced $v_{th} \equiv \sqrt{kT/m}$ as the thermal velocity, i.e. the average velocity of a particle considering only 1 dimension. It should be mentioned that the fraction in front of the temperature is dependent on the degrees of freedom of the particle. A monoatomic particle can only move in three directions, but a diatomic particle can also vibrate and spin.

In high energy plasma physics it is also costumary to drop the Boltzmann factor, k , in eq. (1.1), and express temperature directly in electronvolt, eV. Electronvolt is defined as the energy it takes to move an elementary charge through a potential difference of 1 V, and corresponds to approximately 11600K. For the space and atmospheric plasmas, we are mostly dealing with here, the temperatures are generally low, so we will use the Kelvin scale for temperature.

If the particles in a plasma collide often compared to the characteristic timescales of energy and particle changes, the particle velocity distribution can be approximated by a Maxwellian distribution. It is only then that the concept of temperature is valid (Goldston and Rutherford, 1995).

Electron Plasma Frequency

A rather important frequency in plasma physics is the electron plasma frequency (Chen, 1984),

$$\omega_{pe} \equiv \sqrt{\frac{ne^2}{\epsilon_0 m_e}} \quad (1.2)$$

This frequency, ω_{pe} , is dependent on the number density, n , the fundamental charge, e , the vacuum permittivity, ϵ_0 , and the electron mass, m_e . It can be thought of as a typical electrostatic oscillatory frequency. Consider an electrically neutral 1D slab, which is then disturbed, from its neutrality, by an infinitesimal charge density on one side.

$$\sigma = en\delta x \quad (1.3)$$

It will have an equal and opposite charge density on the other side. The slab will then have an electric field due to the charge density, caused by Gauss' Law.

$$\frac{\partial E_x}{\partial x} = -\frac{\sigma}{\epsilon_0} \quad \rightarrow \quad E_x = \frac{-en\delta x}{\epsilon_0} \quad (1.4)$$

Inserting this field as the only force in Newtons law for a single particle yields

$$m \frac{\partial \delta x}{\partial t} = eE_x = -m\omega_{pe}^2 \delta x \quad (1.5)$$

The particle will then oscillate around its equilibrium position with the electron plasma frequency. The same phenomena often happens in plasma as it tries to go back to its equilibrium and is called plasma oscillations, or Langmuir oscillations, see section 1.5 for a treatment of plasma oscillations.

An otherwise useful timescale is the reciprocal of the plasma frequency, the plasma period

$$\tau_p \equiv 2\pi/\omega_{pe} \quad (1.6)$$

Some researchers prefer to define the τ_p , without the 2π prefactor, as that makes some concepts neater.

Debye Shielding

Debye shielding length is the distance at which the electric influence from a particle is shielded out by the surrounding plasma. Consider a charged particle immersed in a plasma bath. The plasma is in a thermodynamical equilibrium, i.e. there is no significant temperature gradients. We artificially place a positively charged ion into the plasma. This ion will then attract electrons and repel positive ions. There will be a tendency for there to be more negatively charged particles,

and less positive, near the ion, which in effect will work as an electric shield around the ion. The distance away from a particle, where its field is reduced by a factor $1/e$, called the Debye Shielding Length, λ_D .

$$\lambda_D \equiv \sqrt{\frac{\epsilon_0 k T_e}{n_e e^2}} \quad (1.7)$$

The above definition is often used, (Pécseli, 2012), neglecting the ion influence since they often have a much lower temperature. The shielding length is dependent on the ratio between temperature, T_e , and electron density, n_e . In a varmer plasma the particles will move quickly and efficiently shield any charges, so the λ_D becomes smaller. While In cases where we also need to account for ions, a more complete definition can be used

$$\lambda_D \equiv \sqrt{\frac{\epsilon_0 k T_e}{n_e e^2 (1 + Z \frac{T_e}{T_i})}} \quad (1.8)$$

Due to the earlier argument, and the statistical approach used when deriving it (Goldston and Rutherford, 1995), there must be a significant amount particles close to the ion to shield it out.

It should be noted that the shielding length is related (Fitzpatrick, 2014) to the plasma period and the thermal velocity through

$$\lambda_D \omega_{pe} = v_{th} \quad (1.9)$$

Quasineutrality

The assumption of quasi-neutrality is a crucial approximation for collective phenomena in plasma physics. By quasi-neutrality we assume that the electron density is equal to the ion density, $n_e \approx n_i$. This is often called the "*plasma approximation*" (Chen, 1984). This approximation is usually valid on length scales much larger than the shielding length. If we had a case where a large volume of plasma lost a significant amount of charge, a large electric field would accompany the density imbalance. This electric field would quickly correct the imbalance, and quasineutrality would be regained.

Plasma Classification

For a plasma description to be applicable the system we consider must have a typical length scale, L , and time scale, τ , larger than the Debye length and plasma period respectively.

$$\frac{\lambda_D}{L} \ll 1 \quad \frac{\tau_p}{\tau} \ll 1$$

A plasma treatment aims to describe the collective behaviour of many particles. If the length scale is smaller than the λ_D the charges from individual particles are not effectively shielded out and the trajectories of each particle should be considered. On a shorter timescale than the τ_{pe} the plasma oscillation is can be averaged out and needs treatment.

1.2 Single Particle Motion

To better understand the collective motion of plasma it is useful to consider the motions of the single particles that the plasma consists of. By at first treating only one particle we can ignore the electromagnetic influence from the other particles which greatly simplifies the situation. The Lorentz force, eq. (1.10), governs the dynamics of a charged particle in a plasma, provided that other forces, e.g. gravity, are negligible. The Lorentz force is due to charged particles in the electric field, \mathbf{E} , and charged particles moving across the magnetic field \mathbf{B}

$$\mathbf{F} = q(\mathbf{E} + \mathbf{v} \times \mathbf{B}) \quad (1.10)$$

To simplify matters we will only consider particles in static electric and magnetic fields, as that is often a valid approximation on the time and spatial scales of interest.

1.2.1 Gyration

Let us consider a situation with a single moving particle in a static and isotropic external magnetic field, a similar set up as in Baumjohann and Treumann (1997). Newtons Second law together with eq. (1.10) then gives

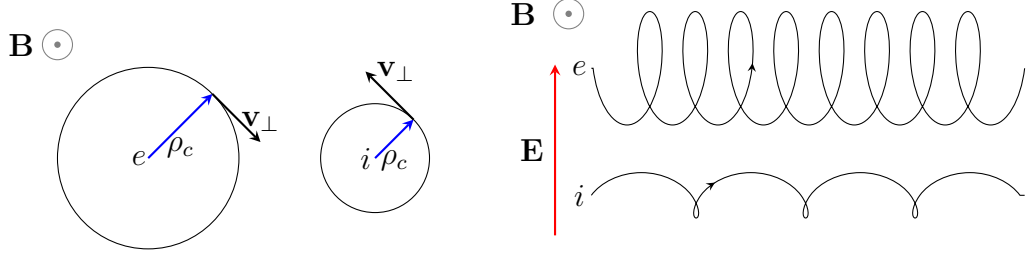
$$m \frac{\partial \mathbf{v}}{\partial t} = q\mathbf{v} \times \mathbf{B} \quad (1.11)$$

We should note that the velocity component parallel to the magnetic field, is not affected by the field and will remain constant, $\frac{\partial \mathbf{v}_{\parallel}}{\partial t} = 0$. The cross product of two parallel vectors is always zero, so $\mathbf{v}_{\parallel} \times \mathbf{B} = 0$. Using these two notions we can write the equation only in terms of the perpendicular, with respect to \mathbf{B} , velocity.

$$m \frac{\partial \mathbf{v}_{\perp}}{\partial t} = q\mathbf{v}_{\perp} \times \mathbf{B} \quad (1.12)$$

Then we perform a temporal derivative.

$$\frac{\partial^2 \mathbf{v}_{\perp}}{\partial t^2} = \frac{q}{m} \frac{\partial \mathbf{v}_{\perp}}{\partial t} \times \mathbf{B} \quad (1.13)$$



(a) The trajectories of an electron, left, and a positive ion, right, is shown (b) Here we can see a particle experiencing the particles trajectory is a gyration encircling the E-cross-B drift. The motion consists of a gyration as well as a constant drift along the x -axis.

Then we insert eq. (1.12) into the equation and use the vector relation $a \times b \times c = b(a \cdot b) - c(a \cdot b)$.

$$\frac{\partial^2 \omega_\perp}{\partial t^2} + \left(\frac{qB}{m} \right)^2 \omega_\perp = 0 \quad (1.14)$$

In the last equation we also changed the term describing the rotational motion to ω_\perp , which will from now on signify gyroscopic motion. This differential equation corresponds to a gyration around the magnetic field lines with the gyration frequency, $\omega_c = \frac{qB}{m}$, as the frequency. The particles are free to move parallel to the magnetic field lines causing a spiralling motion along the magnetic field lines, as illustrated in fig. 1.2a. This spiral effect is often an important part of why there are often field-aligned currents, such as 'Birkeland Currents' (Cummings and Dessler, 1967), transporting plasma along magnetic field lines.

1.2.2 E-cross-B Drift

A drift called E-cross-B drift can appear when a particle is moving within static and isotropic electric and magnetic fields. The equation of motion, neglecting all forces except the electromagnetic, is then

$$m \frac{\partial \mathbf{v}}{\partial t} = q(\mathbf{E} + \mathbf{v} \times \mathbf{B}) \quad (1.15)$$

In plasma physics it is often a good strategy to decompose quantities into parallel and perpendicular, with respect to \mathbf{B} , quantities. We start by separating the velocity into $\mathbf{v} = \mathbf{v}_\parallel + \mathbf{v}_\perp$ and the electric field into $\mathbf{E} = \mathbf{E}_\parallel + \mathbf{E}_\perp$. Inserting this and using that $\mathbf{v}_\parallel \times \mathbf{B} = 0$ again the equation becomes

$$m \frac{\partial}{\partial t} (\mathbf{v}_\parallel + \mathbf{v}_\perp) = q (\mathbf{E}_\perp + \mathbf{E}_\parallel + (\mathbf{v}_\perp) \times \mathbf{B}) \quad (1.16)$$

The parallel motion consist of an acceleration caused by the parallel part of the electric field and is given by

$$m \frac{\partial \mathbf{v}_{\parallel}}{\partial t} = q \mathbf{E}_{\parallel} \quad (1.17)$$

The remaining part of the equation describes the perpendicular motion.

$$m \frac{\partial \mathbf{v}_{\perp}}{\partial t} = q (\mathbf{E}_{\perp} + (\mathbf{v}_{\perp}) \times \mathbf{B}) \quad (1.18)$$

Now we assume there is a time-invariant drift \mathbf{v}_D , i.e. not dependent on time, and then we separate the perpendicular motion into a drift and gyration, $\mathbf{v} = \mathbf{v}_{\parallel} + \boldsymbol{\omega}_{\perp} + \mathbf{v}_D$.

$$m \frac{\partial}{\partial t} (\boldsymbol{\omega}_{\perp} + \mathbf{v}_D) = q (\mathbf{E}_{\perp} + (\boldsymbol{\omega}_{\perp} + \mathbf{v}_D) \times \mathbf{B}) \quad (1.19)$$

From section 1.2.1 we know that the gyration part is given by

$$m \frac{\partial \boldsymbol{\omega}_{\perp}}{\partial t} = q \boldsymbol{\omega}_{\perp} \times \mathbf{B} \quad (1.20)$$

Taking this out of the equation we have

$$\frac{\partial \mathbf{v}_D}{\partial t} = \frac{q}{m} (\mathbf{E}_{\perp} + \mathbf{v}_D \times \mathbf{B}) \quad (1.21)$$

Then we use the previous assumption that the drift velocity is constant, cross the equation with \mathbf{B} and simplify, see Goldston and Rutherford (1995), to arrive at

$$\mathbf{v}_D = \frac{\mathbf{E} \times \mathbf{B}}{B^2} \quad (1.22)$$

As we can see the E-cross-B drift is independent of particle charge and mass, which means both the ions and electrons will be drifting in the same direction and speed perpendicular to the electric and magnetic fields, fig. 1.2b.

This is an example of some effects on single particle motion in electric and magnetic fields, and there are many other important concepts found in considering single particles, that we will not go into here, see Fitzpatrick (2014), or other introductory plasma physics book. Other examples that could be useful to know about is gradient-B drift, curvature drift, polarization drift and magnetic mirroring. The motions of single particles are necessary to understand the collective behaviour of large amounts of particles constituting a plasma.

1.3 Kinetic Theory

Here we will shortly introduce kinetic theory in relation to plasma physics. To consider a large amount of particles we consider a charge and current density instead of the individual particles. Let \mathcal{F}_s be the exact phase-space density of a particle species, it contains all the positions, velocities for all the particles at all times. By integrating over all velocities and multiplying with the charge for all species we obtain the charge density, ρ_c .

$$\rho_c = \sum_s e_s \int \mathcal{F}_s(\mathbf{r}, \mathbf{v}, t) d^3\mathbf{v}$$

Likewise we find the current density, \mathbf{j} by:

$$\mathbf{j} = \sum_s e_s \int \mathbf{v} \mathcal{F}_s(\mathbf{r}, \mathbf{v}, t) d^3\mathbf{v}$$

Then it seems we can derive all plasma interaction from considering the conservation of the phase-space density, coupled with Maxwell's equations. The phase-space conservation is given by what is known as Vlasov's equation eq. (1.23) (Pécseli, 2012)).

$$\frac{\partial \mathcal{F}}{\partial t} + \mathbf{v} \cdot \nabla \mathcal{F}_s + \frac{e_s}{m_s} (\mathbf{E} + v \times \mathbf{B}) \cdot \nabla_v \mathcal{F}_s = 0 \quad (1.23)$$

where ∇_v is the velocity grad-operator. Unfortunately this expression, combined with Maxwell's equations, is only solvable for special simple geometries.

1.4 Fluid Description

This section aims to provide an overview of the derivation of the fluid equations from a Kinetic Theory perspective. First the Vlasov equation is introduced, then it is explained how the fluid equations can be obtained by taking different order moments of the Vlasov equation. This can help understand the limitations of the fluid model of plasma. Lastly a few different approximations are introduced to make the fluid equations closable.

1.4.1 Velocity Moments

To investigate plasma as a fluid we have to make certain fluid approximations. The plasma is then characterized by local parameters describing particle density, kinetic temperature, flow velocity and so on. These parameters refer to a small volume of plasma, in contrast with the discussions earlier about single particle

motion, section 1.2. The time evolution is then governed by the fluid equation, but unfortunately the resulting equations are generally less tractable than the usual hydrodynamical equations. This is due to the need to close them with Maxwell's equations.

The first order moment is given by mass times velocity, in introductory physics literature this is usually referred to as the moment. Here we will introduce a more general form of moment. This will help understand how the fluid equations result from averaging over different moments of the general transport equation. The zeroth, first and second order moment is respectively given by

$$\Phi^0(\mathbf{v}) = m \quad (1.24a)$$

$$\Phi^1(\mathbf{v}) = m\mathbf{v} \quad (1.24b)$$

$$\Phi^2(\mathbf{v}) = m\mathbf{v}\mathbf{v} \quad (1.24c)$$

By integrating the moment functions and the distribution function \mathcal{F} , over the velocity space we can retrieve different quantities.

Integrating the zeroth order moment gives the density, if we divide by the mass.

$$n = \frac{1}{m} \int m\mathcal{F}d\mathbf{v} \quad (1.25)$$

Integrating over the first order moment gives the momentum, if we divide by density.

$$m\mathbf{v} = \int m\mathbf{v}\mathcal{F}d\mathbf{v} \quad (1.26)$$

We can in fact find the mean of any order moment by integrating the distribution function over \mathcal{F} .

$$\langle \Phi^n(\mathbf{v}) \rangle = \frac{1}{n} \int \Phi^n \mathcal{F} d\mathbf{v} \quad (1.27)$$

1.4.2 Transport Equation

By multiplying the moment function, Φ , with the Vlasov equation, eq. (1.23), we obtain the general momentum transport equation (Shu, 2010).

$$\frac{\partial n \langle \Phi^n(\mathbf{v}) \rangle}{\partial t} + \nabla \cdot (\langle \Phi^n(\mathbf{v}) \mathbf{v} \rangle) = \frac{n}{m} \langle \mathbf{F}_L \cdot \nabla_v \Phi^n(\mathbf{v}) \rangle \quad (1.28)$$

This then becomes a conservation equation for the average macroscopic quantity $\langle \Phi \rangle$. By multiplying this equation with the moments the fluid equations can be obtained, see section 1.4.3.

1.4.3 Fluid Equations

From the Vlasov equation and the zeroth, first and second order moment we obtain the fluid equations. The generalized fluid equations is given in eqs. (1.29a) to (1.29c), where the three equations describe the conservation of mass, momentum and energy respectively. The collision term is neglected. We refer to Fitzpatrick (2014), although some notation differ, for the rather involved derivation to obtain these equations.

$$\left(\frac{\partial}{\partial t} + \mathbf{u}_s \cdot \nabla \right) n_s + n_s \nabla \cdot \mathbf{u}_s = 0 \quad (1.29a)$$

$$m_s n_s \left(\frac{\partial}{\partial t} + \mathbf{u}_s \cdot \nabla \right) \mathbf{u}_s = -\nabla p_s - \nabla \cdot \boldsymbol{\pi} + n_s \mathbf{f}_s \quad (1.29b)$$

$$\left(\frac{\partial}{\partial t} + \mathbf{u}_s \cdot \nabla \right) p_s = -\frac{5}{3} p_s \nabla \cdot \mathbf{u}_s - \frac{2}{3} \boldsymbol{\pi}_s : \nabla \mathbf{u}_s - \frac{2}{3} \nabla \cdot \mathbf{q}_s \quad (1.29c)$$

The first equation, eq. (1.29a), is the continuity equation, it states that the total mass in a volume should be preserved. \mathbf{u}_s is the flow velocity and n_s is the number density, i.e. number of particles in a volume. The divergence terms signify change due to the compressability of the fluid and can in many cases be set to 0. The total derivative, i.e. $(\frac{\partial}{\partial t} + \mathbf{u}_s \cdot \nabla)$ accounts for change in density in a volume taking into account substance exiting and entering. The momentum equation eq. (1.29b) shows that the fluid momentum change, left hand side, is due to pressure gradients, ∇p_s , viscous forces, $\nabla \cdot \boldsymbol{\pi}$ and external forces, $n_s \mathbf{f}_s$, per unit volume. Lastly we have the energy equation, in its pressure form, which shows that changes to thermal energy, $p = nkT$, are caused by compression, $p_s \nabla \cdot \mathbf{u}_s$, viscous effects $\boldsymbol{\pi}_s : \nabla \mathbf{u}_s$ and heat transport $\frac{2}{3} \nabla \cdot \mathbf{q}_s$. The fluid equations are in general not closeable and adding higher order moments always introduces more unknowns. Due to this one generally uses different closing schemes to make them tractable. Some of these schemes are described in the next section.

1.4.4 Plasma States

Plasma can be classified according to which approximations and simplifications that are valid for them. Here we will go through some of the most used approximations.

Local Thermodynamic Equilibrium

A plasma is said to be in a *local thermodynamic equilibrium* (LTE) if the phase-space distribution is locally Maxwellian. This means the variations in temperature are slow enough that we can neglect heat conduction in the plasma. We can

also ignore the viscosity due to there being little local variations to the momentum flow.

$$\mathcal{F}_m = \frac{n}{(2\pi)^{3/2}v_t^3} \exp\left\{-\frac{(v-u)^2}{2v_t^2}\right\} \quad (1.30)$$

Since the viscosity tensor, π , and the heat flux tensor, \mathbf{q} contains odd integrals over the distribution, see Fitzpatrick (2014), they disappear.

Cold Plasma

In a cold plasma the temperature is assumed to be 0, this causes the pressure, p , and viscosity, π , to be zero. This can be useful if the velocities of interest far exceed the thermal velocities.

Isothermal

An isothermal plasma is one where we assume an infinite heat conductivity, this means the temperatures is constant in all space and time. This can be used to describe macroscopic plasma. (ADD MORE)

1.5 Plasma Oscillations

Plasma oscillations, also called Langmuir oscillations, is the basic resulting oscillation that happens as a plasma tries to reach a stable equilibrium, due to a small perturbation of its density. We will use this to show how the fluid equations can be closed for a simple system using assumptions. This is also very suited to test simulations, as we do later in section 5.2.1.

Here we will consider an one specie plasma fluid consisting of electrons under local thermal equilibrium, LTE. The electron density, n_0 and pressure, p_0 , is initially homogenous. The fluid has a vanishing flow, $\mathbf{u}_0 = 0$, and no initial potential gradient $\phi_0 = 0$. The ele See Pécseli (2012) for a another discussion.

A small perturbation of the electron density will cause the electric field to try to restore the equilibrium. When the electrons reach the equilibrium position they will have a kinetic energy and will overshoot. This will cause a new perturbation away from the equilibrium.

Under the LTE conditions the fluid equations simplify to

$$\frac{\partial n_e}{\partial t} + \nabla \cdot (n_e \mathbf{u}_e) = 0 \quad (1.31a)$$

$$m_e n_e \left(\frac{\partial}{\partial t} + \mathbf{u}_e \cdot \nabla \right) \mathbf{u}_e = e n_e \nabla \phi - \nabla p_e \quad (1.31b)$$

$$\left(\frac{\partial}{\partial t} + \mathbf{u}_e \cdot \nabla \right) p_e + \frac{5}{3} p_e \nabla \cdot \mathbf{u}_e = 0 \quad (1.31c)$$

Since this set of equations have more unknowns than equations so we need additional information to close the set. Here we can use the Poisson equation to close it.

$$\epsilon_0 \nabla^2 \phi = e(n_e - n_0) \quad (1.32)$$

Now we let a small perturbation, denoted by a tilde, happen to the equilibrium. Since we are free to choose an inertial reference frame, we select one co-moving with the plasma so the initial fluid velocity is $\mathbf{u}_0 = 0$. We also select the reference potential so the initial potential, ϕ_0 , is 0.

$$\text{Perturbation} \rightarrow \begin{cases} n_e = n_0 + \tilde{n}_e \\ p_e = p_0 + \tilde{p}_e \\ \mathbf{u}_e = \tilde{\mathbf{u}}_e \\ \phi = \tilde{\phi} \end{cases}$$

Since the perturbation is small, we can say that any part that contains second order terms of perturbation of a quantity will be much smaller than the value of the quantity, $q \gg \tilde{q}\tilde{q}$. So even though we may miss some processes by doing this, we can drop the second order perturbation terms. This process is called linearization.

Inserting the perturbation and linearizing the equations we get:

$$\frac{\partial \tilde{n}_e}{\partial t} + \nabla \cdot (n_0 \tilde{\mathbf{u}}_e) = 0 \quad (1.33a)$$

$$m_e \frac{\partial \tilde{\mathbf{u}}_e}{\partial t} = e \nabla \tilde{\phi} - \frac{\nabla \tilde{p}_e}{n_0} \quad (1.33b)$$

$$\frac{\partial \tilde{p}_e}{\partial t} + \frac{5}{3} p_0 \nabla \cdot \tilde{\mathbf{u}}_e = 0 \quad (1.33c)$$

$$\epsilon_0 \nabla^2 \tilde{\phi} = e \tilde{n}_e \quad (1.33d)$$

Then we combine the continuity and energy equations, eq. (1.33a) and eq. (1.33c).

$$\frac{\partial}{\partial t} \left(\frac{\tilde{p}_e}{p_0} + \frac{5}{3} \frac{\tilde{n}_e}{n_0} \right) = 0 \quad (1.34)$$

The perturbed pressure and density are proportional, $\nabla \tilde{p}_e = (5p_0/3n_0) \nabla \tilde{n}_e$. Assuming plane wave solutions along the x-axis, the differential operators become $\nabla \rightarrow ik$ and $\frac{\partial}{\partial t} \rightarrow -i\omega$, we can solve for the dispersion relation.

$$\epsilon(\omega, k) = 1 + \frac{5}{3} \lambda_{se}^2 k^2 - \frac{\omega^2}{\omega_{pe}^2} \quad (1.35)$$

Here the electron debye length, λ_D , and the plasma frequency, ω_{pe} , have been inserted.

1.6 Magnetohydrodynamics

In a plasma there are usually several types of species, then it follows that each specie needs its own set of fluid equations. Magnetohydrodynamics, (MDH), is an attempt to simplify this situation by combining it into one electrically conducting fluid. Conventional MHD assumes local thermodynamical equilibrium, negligible electron inertia and quasi-neutrality (Goldston and Rutherford, 1995). This simplifies Maxwell's equations to

$$\nabla \times \mathbf{B} = \mu_0 \mathbf{j} \quad (1.36a)$$

$$\nabla \times \mathbf{E} = -\frac{\partial \mathbf{B}}{\partial t} \quad (1.36b)$$

$$\nabla \cdot \mathbf{B} = \nabla \cdot \mathbf{E} = 0 \quad (1.36c)$$

The MHD fluid can be considered a neutral fluid with a current running through it (Hockney and Eastwood, 1988). The current is described by the conductivity σ and the bulk velocity \mathbf{v} and is given as

$$\mathbf{j} = \sigma \mathbf{v} \quad (1.37)$$

With the condition that the conductivity is high and a finite current eq. (1.36b) becomes

$$\frac{\partial \mathbf{B}}{\partial t} = \nabla \times (\mathbf{v} \times \mathbf{B}) \quad (1.38)$$

Then it remains to close the MHD equations by continuity and momentum conservation, where ρ is the mass density and p is the scalar pressure.

$$\frac{\partial \rho}{\partial t} = \nabla \cdot (\rho \mathbf{v}) \quad (1.39a)$$

$$\rho \frac{\partial \mathbf{v}}{\partial t} = -\nabla p + \mathbf{j} \times \mathbf{B} \quad (1.39b)$$

1.7 Numerical Simulations

The mathematical description of plasma is helpful to improve our understanding of the physics, many problems doesn't fall neatly into convenient assumptions or are untractable. Then we need to turn to experiments and computer simulations solve them. All of these methods work in symbiosis and is interdependent on each other. Numerical simulations bears many similarities to experiments, but

it also has the advantage of being applied to situations that no experiment can reproduce. In addition physical experiments often has constraints on what can be measured directly, while numerical experiments have all the wanted data readily available. Modelling generally needs to be validated against experiments and has a foundation built upon theory. As the computational resources have improved, more sophisticated simulations have been possible. Plasma simulations vary from fluid descriptions, as MHD codes, to kinetic descriptions, as Particle-in-Cell and Vlasov codes, with hybrid codes inbetween as well. This thesis focuses on the development of a Particle-in-Cell code, but here we will give a brief overview of other modelling approaches as well.

MHD

Magnetohydrodynamical codes solve the one-fluid equations, given in section 1.6, with various approaches and has similarities to Computational Fluid Dynamics. For the fluid equations to be a reasonable description of plasma, the dynamics needs to happen at much larger scales than the Debye Shielding Length. This approach has been widely used in large scale plasma simulations such as astrophysics, see Hawley and Stone (1995) where an MHD approach is discussed with regards to astrophysical problems, and space physics, see Watanabe and Sato (1990) for an investigation of the solar wind-magnetsphere interaction.

Particle-in-Cell

Particle-in-Cell models the particles directly, this has the advantage that few approximations are done, but computational increases fast with more particles. Numerical PiC codes has been used extensively to research charging- and wake-effect on spacecraft operating in the upper earth atmosphere ().

Vlasov

Vlasov codes takes the kinetic description as the starting point and are often used in plasma laser modelling (Bertrand et al., 1990). It has an advantage over PiC in low density zones, where there is often too few particles for PiC.

Chapter 2

Method

(REWRITE)

As the previous chapter described the need for numerical plasma models this chapter goes through the theory behind a Particle-In-Cell model, with a focus on multigrid as a Poisson solver. First there is a general overview of a PiC model and the different building blocks needed. Then there is an overview of the normalization scheme designed to minimize floating point operations, FLOPS. Domain partitioning as a strategy to parallelize the model is then considered. How the multigrid solver works and is structured follows, before the parallelization issues for the multigrid solver are considered. Lastly there is an overview of boundary conditions and the special considerations they have in a multigrid solver.

2.1 Particle-in-Cell

Particle based plasma simulations have been in use since the 1960s, (Verboncoeur, 2005), and part of this project was to design a massively parallel implementation, with a focus on the Poisson solver. The aim of this chapter is to describe simple and fast PiC model, with good scaling properties, as a baseline and rather add in extra functionality later. Due to this it uses an electrostatic model and ignores relativistic effects, which makes it faster and more suited to certain tasks, such as space plasmas and plasma discharges. For an example of a modern relativistic full electromagnetic model see Sgattoni et al. (2015).

The first particle based plasma calculations was done by Dawson, 1962 and Buneman (1959). They computed the electrical force directly between the particles leading to a computational scaling of $\mathcal{O}((\# \text{particles})^2)$. Since a large number of particles is often wanted the PiC method seeks to improve the scaling by computing the force on the particles from an electric field instead. The electric field is computed from the charge distribution obtained from the plasma particle distribution. For an electrostatic model, which this thesis focuses on, this is usually done by solving the Poisson equation, eq. (2.1), over the whole domain,

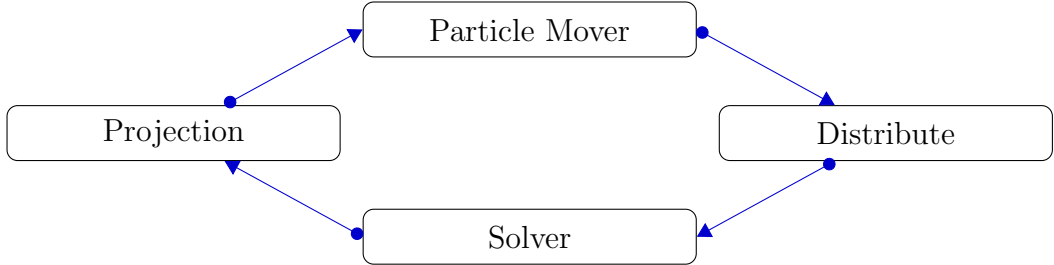


Figure 2.1: Schematic overview of the PIC cycle. The mover moves all the particles and updates the velocities. Next the charges are distributed to a charge density grid by a distribute algorithm. The solver then obtains the electric field, and magnetic field in a full electromagnetic model. Lastly the field values are projected onto the particles.

Ω . The input to the solver is the charge density, ρ , and the output is the potential, ϕ .

$$\nabla^2\phi = -\rho \quad \text{in} \quad \Omega \quad (2.1)$$

A PiC model has 4 main components: the mover, the weighting scheme, the field solver and the distributor. See fig. 2.1 for an overview of the PiC cycle. The mover is responsible for moving the particles and updating the velocities of the particles. The distribute module computes a charge distribution from the particle distribution, This is often done with 1st order interpolation, resulting in second order accuracy. Different order interpolation can also be used. The solver then computes the electric field. For an electrostatic case a multigrid algorithm is often used but there described in section 2.1.2. Lastly the fields are projected onto the particles.

2.1.1 Movers

The mover in a PiC model has the task of moving all the particles according to the velocity of the particles, as well as the electric and magnetic fields. An often used mover is the *Leapfrog* algorithm (Birdsall and Langdon, 2004), derived from a forward finite difference discretization of the timestep. Then the velocity is shifted half a timestep forward improving the accuracy, with no extra computations needed compared with *Euler* integration. When the magnetic force also needs to be considered the most used algorithm is the *Boris* algorithm (Qin et al., 2013), employing rotations to efficiently deal with the cross product. While the aforementioned movers are explicit, based on a forward discretization of the time, implicit algorithms are also well developed (Friedman et al., 1981), although not covered here. Implicit algorithms impose less restrictions on the choice of the spatial resolution.

2.1.2 Field Solvers

The Poisson equation, ??, is a well known and investigated problem. Here we will mention some advantages and disadvantages of different possible field solvers before we describe our choice of a multigrid solver.

Spectral Methods

(NOTE TO SELF: Shen no fourier transform, find different source, Name what A and B are.) The spectral methods is based on rewriting the problem into a sum of bases functions frequencies and solving the problem on the basis functions form, see Israeli and Sherman (2005) for an implementation of an spectral Poisson solver. Often the basis functions chosen are sinusoidal, allowing the Fourier Transform to be used. Other basis functions can also be used as in Shen (1994). They are efficient solvers that can be less intricate to implement, but can be inaccurate for complex geometries.

When looking for a solution with a spectral method we first rewrite the problem in the form of the basis functions, in this case sinusoids, which for the three-dimensional Poisson equation would be

$$\nabla^2 \sum A_{j,k,l} e^{i(jx+ky+lz)} = \sum B_{j,k,l} e^{i(jx+ky+lz)} \quad (2.2)$$

where $A_{j,k,l}$ and $B_{j,k,l}$ are the coefficients of the sinusoids. From there we get a relation between the coefficients

$$A_{j,k,l} = -\frac{B_{j,k,l}}{j^2 + k^2 + l^2} \quad (2.3)$$

Then we compute the Fourier transform of the right hand side obtaining the coefficients $B_{j,k,l}$. We compute all the coefficients $A_{j,k,l}$ from the relation between the coefficients. At last we perform a inverse Fourier transform of the left hand side obtaining the solution.

$$(2.4)$$

Finite Element Methods

The finite element (FEM) is a method to numerically solve a partial differential equations (PDE) first transforming the problem into a variational problem and then constructing a mesh and local trial functions, see Alnæs et al., 2011 for a more complete discussion. FEM is similar to a spectral solver, with the main difference that FEM's basis functions are only locally nonzero.

To transform the PDE to a variational problem we first multiply the PDE by a test function v , then it is integrated using integration by parts on the second

order terms. Then the problem is separated into two parts, the bilinear form $a(u, v)$ containing the unknown solution and the test function, as well as the linear form $L(v)$ containing only the test function.

$$a(u, v) = L(v) \quad v \in \hat{V} \quad (2.5)$$

Next we construct discrete local function spaces of that we assume contain the trialfunctions and testfunctions. The function space, \hat{V} , often consists of locally defined functions that are 0 except in a close neighbourhood of a mesh point, so the resulting matrix to be solved is sparse and can be computed quickly. The matrix system is then solved by a suiting linear algebra algorithm, before the solution is put together. The FEM method is very suited to tackling problems on complicated grids.

Multigrid

The multigrid method used to solve the Poisson equation and obtain the electric field is a widely used and highly efficient solver for elliptic equations, having a theoretical scaling of $\mathcal{O}(N)$ (Press et al., 1988), where N is the number of grid points. It is very well suited to simple geometries that can easily be translated to coarser problems. Due to this it we have chosen to use it as the solver in our PiC model. The multigrid method is based on iterative solvers such as Gauss-Seidel, section 2.5.2, these have the property that they quickly eliminate local errors in the solution, while far away influences takes longer to incorporate. Multigrid algorithms tries to lessen this problem by transforming this problem to a coarser grid so the distant errors gets solved in fewer iterations. Due to this it needs algorithms to transfer the problem between coarser and finer grids, which is called restrictors and prolongators. The multigrid algorithm is described in more detail in section 2.5.

2.2 Stability

A numerical model often has numerical stability criterias that need to be fulfilled for the model to work. This is caused by the inherent discretization of the problem in a numerical method. Here we will investigate an harmonic oscillator and a wave to find the stability criterias for the time and spatial discretization.

2.2.1 Time Stability Criterion

A one-dimensional harmonic oscillator, i.e. a pendulum in gravity, is described by

$$\frac{\partial^2 x}{\partial t^2} = -\omega_0^2 x \quad (2.6)$$

and has a solution of the form

$$x(t) = Ce^{-i\omega t} \quad (2.7)$$

Then we replace the temporal derivative with a centered finite difference.

$$\frac{x^{n+\Delta t} - 2x^n + x^{n-\Delta t}}{\Delta t^2} = -\omega_0^2 x^n \quad (2.8)$$

Inserting the harmonic solution in place of the x^n , $x^{n+\Delta t}$ and $x^{n-\Delta t}$.

$$\frac{e^{-i\omega(t+\Delta t)} - 2e^{-i\omega t} + e^{-i\omega(t-\Delta t)}}{\Delta t^2} = -\omega_0^2 e^{-i\omega t} \quad (2.9)$$

Using Eulers relation, ($e^{-ix} = \cos(x) + i \sin x$), this yields

$$2 \cos(\omega \Delta t) - 2 = -\omega_0 \Delta t \quad (2.10)$$

which can be reshuffled to

$$\sin\left(\frac{\omega \Delta t}{2}\right) = \pm \frac{\omega_0 \Delta t}{2} \quad (2.11)$$

In the case, $\frac{\omega_0 \Delta t}{2} > 1$, ω has an imaginary component and the numerical solution is unstable.

2.2.2 Spatial Stability Criterion

A 1-dimensional wave equation is described by:

$$\frac{\partial^2 \varphi}{\partial t^2} = c^2 \frac{\partial \varphi}{\partial x} \quad (2.12)$$

Applying a centered difference

$$\frac{\varphi_j^{n+\Delta t} - 2\varphi_j^n + \varphi_j^{n-\Delta t}}{\Delta t^2} = c^2 \frac{\varphi_{j+\Delta x}^n - 2\varphi_j^n + \varphi_{j-\Delta x}^n}{\Delta x^2} \quad (2.13)$$

Let us assume sinusoidal waves, $\varphi_j^n = e^{i(\omega t - \tilde{k}j\Delta x)}$.

$$\frac{e^{i\omega \Delta t} - 2 + e^{-i\omega \Delta t}}{\Delta t^2} = c^2 \frac{e^{-i\tilde{k}\Delta x} - 2 + e^{i\tilde{k}\Delta x}}{\Delta x^2} \quad (2.14)$$

Which can be rewritten to

$$\cos(\omega \Delta t) = \left(c \frac{\Delta t}{\Delta x}\right)^2 \left(\cos(\tilde{k}\Delta x) - 1\right) + 1 \quad (2.15)$$

ω needs an imaginary part if $(c \frac{\Delta t}{\Delta x})^2 > 1$, this is called the *Courant-Lewy Stability criterion* (Courant et al., 1869). In general for more dimensions it becomes

$$\Delta t \leq \frac{1}{c} \left(\sum_i \Delta x_i^{-2} \right)^{-\frac{1}{2}} \quad (2.16)$$

2.2.3 Finite Grid Instability

The particles in a PiC simulation moves in a continuous space, while they are represented on a discrete grid for the field calculations. This reduction allows a *Finite Grid Instability* to appear, due to a loss of information (Lapenta, 2016). The numerical analysis of the instability is complicated and we refer to Birdsall and Langdon (2004) and Hockney and Eastwood (1988) for a complete picture. The instability introduces the following additional constraint on the grid resolution,

$$\Delta x < \varsigma \lambda_D \quad (2.17)$$

For a CiC

2.3 Normalization

For most numerical code significant computational gains can be achieved relatively easy by smart normalization. With a succesful normalization most of the multiplications with constants will dissappear. Numerical errors due to machine precision are smallest close to unity, $\mathcal{O}(1)$, (Hjorth-Jensen, 2016) so we want to work with numbers as close to unity as we can. As a sidebenefit it also makes the code easier to write and cleaner to read. Consider a single particle, with mass m and charge q , in an electric field \mathbf{E} . Its equation of motion is then

$$m \frac{\partial^2 \mathbf{r}}{\partial t^2} = q \mathbf{E} \quad (2.18)$$

To compute the acceleration of this particle completely naive would at each point cost 1 multiplications and 1 division, $m/q * E$. If we instead use smartly normalized values the equation could look like this

$$\frac{\partial^2 \tilde{\mathbf{r}}}{\partial t^2} = \tilde{\mathbf{E}} \quad (2.19)$$

where $\tilde{\mathbf{r}}$ and $\tilde{\mathbf{E}}$ is normalized so the dimensionality of the equation works out. Here we get away with no multiplications and no divisions, but we do have the added task of transforming our variables first to the normalized variables and then back to the original after the simulation has run.

2.3.1 Non-dimensionality PinC

A good dimensionalizing strategy is to first remove dimensionality from the fundamental quantities, and then work out the normalizations necessary for the derived quantities.

The fundamental quantities that are involved in our PiC simulation is mass m , position \mathbf{r} , time t and charge q . Since we are dealing with plasma it is useful to normalize with Debye-length, λ_D , and electron plasma frequency, ω_{pe} . The normalized quantities are then:

$$\tilde{\mathbf{r}} = \frac{\mathbf{r}}{\lambda_D} \quad (2.20a)$$

$$\tilde{t} = \omega_{pe} t \quad (2.20b)$$

$$\tilde{m} = \frac{m}{m_e} \quad (2.20c)$$

$$\tilde{q} = \frac{q}{e} \quad (2.20d)$$

Next we need the velocity, which is the temporal derivative of the position. This is normalized by transforming the position to the nondimensional position, by eq. (2.20a), as well as changing the temporal derivative to a nondimensional temporal, by eq. (2.20b).

$$\frac{\partial \mathbf{r}}{\partial t} = v \rightarrow \frac{\partial \tilde{\mathbf{r}}}{\partial \tilde{t}} = \tilde{\mathbf{v}} = \frac{\mathbf{v}}{v_{th}} \quad (2.21)$$

Here we have introduced the thermal velocity, mentioned in section 1.1.1, $v_{th} = \lambda_{De}\omega_{pe}$.

Now we will use the Lorentz force to normalize the electromagnetic fields.

$$\frac{\partial \mathbf{v}}{\partial t} = \frac{q}{m} (\mathbf{E} + \mathbf{v} \times \mathbf{B}) \quad (2.22)$$

Swapping in all the nondimensional values from eqs. (2.20a) to (2.20d) we obtain

$$\frac{\partial(\tilde{\mathbf{v}}v_{th})}{\partial(\tilde{t}/\omega_{pe})} = \frac{(\tilde{q}e)}{(\tilde{m}m_e)} (\mathbf{E} + (\mathbf{v}v_{th}) \times \mathbf{B}) \quad (2.23)$$

$$\frac{\partial \tilde{\mathbf{v}}}{\partial \tilde{t}} = \frac{\tilde{q}}{\tilde{m}} \left(\frac{e}{v_{th}\omega_{pe}m_e} \mathbf{E} + \tilde{\mathbf{v}} \times \frac{e}{\omega_{pe}m_e} \mathbf{B} \right) \quad (2.24)$$

This suggests that we use the following nondimensionalized fields

$$\tilde{\mathbf{E}} = \frac{e}{v_{th}\omega_{pe}m_e} \mathbf{E} \quad \text{and} \quad \tilde{\mathbf{B}} = \frac{e}{\omega_{pe}m_e} \mathbf{B} \quad (2.25)$$

The electric field is related to the charge density ρ through Gauss' law.

$$\nabla \cdot \mathbf{E} = \frac{\rho}{\epsilon_0} \quad (2.26)$$

Inserting normalized quantities for \mathbf{E} and the gradient operator

$$\tilde{\nabla} = \left(\frac{\partial}{\partial \tilde{x}}, \frac{\partial}{\partial \tilde{y}}, \frac{\partial}{\partial \tilde{z}} \right) = \lambda_D \nabla \quad (2.27)$$

$$\frac{1}{\lambda_D} \tilde{\nabla} \cdot \frac{v_{th} \omega_{pe} m_e}{e} \tilde{\mathbf{E}} = \frac{\rho}{\epsilon_0} \quad (2.27)$$

$$\tilde{\nabla} \cdot \tilde{\mathbf{E}} = \frac{\lambda_D e}{v_{th} \omega_{pe} m_e} \frac{\rho}{\epsilon_0} \quad (2.28)$$

This gives the dimensionless charge density

$$\tilde{\rho} = \frac{\rho}{n_0 e} \quad (2.29)$$

2.3.2 Normalization PinC

It should be mentioned that the normalization scheme for PinC was mostly worked out by Sigvald Marholm, and I am mostly repeating his work here. It is still included here to give complete understanding of our PiC implementation. The general aim of the normalization scheme is to reduce the number of floating point operations on the particles. Since there are usually fewer grid points, i.e. values for fields such as ρ and \mathbf{E} , than particles in a simulation a multiplication should preferably be done to a field instead of each particle. From now on we will omit the $\tilde{\cdot}$ on dimensionless quantities and consider all quantities dimensionless.

2.3.3 Mover

We use the Leapfrog algorithm from *Plasma Physics via Computer Simulation* (Birdsall and Langdon, 2004) book. This has the perks of second order accuracy and stability for oscillatory motion with the same number of function calls as Euler integration. It should be mentioned that the Leapfrog algorithm preserves momentum, but the energy can drift.

The finite-difference discretization of a leapfrog step is given by

$$\frac{\mathbf{r}^{n+1} - \mathbf{r}^n}{\Delta t} = \mathbf{v}^{n+\frac{1}{2}} \quad (2.30)$$

By discretizing time as $\bar{t} = t/\Delta t$ and the position and velocity as

$$\bar{\mathbf{r}} = \left(\frac{x}{\Delta x}, \frac{y}{\Delta y}, \frac{y}{\Delta y} \right) \quad (2.31)$$

$$\bar{\mathbf{v}} = \Delta t (\delta \mathbf{r})^{-1} \mathbf{v} \quad (2.32)$$

we obtain the simpler step equation

$$\bar{\mathbf{r}}^{n+1} = \bar{\mathbf{r}}^n + \bar{\mathbf{v}}^{n+\frac{1}{2}} \quad (2.33)$$

2.3.4 Accelerator

The accelerator sets a new velocity to the particles. For an case with no magnetic field the equation of motion becomes

$$\frac{\partial \mathbf{v}}{\partial t} = \frac{q_s}{m_s} \mathbf{E} \quad (2.34)$$

Discretizing the equation and normalizing the electric field as

$$\bar{\mathbf{E}} = \frac{\Delta t^2}{\Delta \mathbf{r}} \frac{q_0}{m_0} \mathbf{E} \quad (2.35)$$

the velocity step for a particle species is given by

$$\bar{\mathbf{v}}^{n+\frac{1}{2}} = \bar{\mathbf{v}}^{n-\frac{1}{2}} + \xi_s \xi_{s-1} \cdots \xi_1 \bar{\mathbf{E}} \quad (2.36)$$

where the specie specific normalization coefficient is:

$$\xi_s = \frac{q_s/m_s}{q_{s-1}/m_{s-1}} \quad (2.37)$$

By applying the cooefficient directly to the electric field this enables us to accelerate each particle with 1 addition.

2.3.5 Distribute

The interpolation of the charged particles onto a charge density grid is handled by the distribute module. For each particle the charge is distributed to the nearby grid points according distance. We will not go into the details of the implementation here, only mention the resulting normalization.

The normalized charge density at grid point j is given by adding together the contribution from each particle species

$$\bar{\rho}_j = \sum_i \omega_{ij} \bar{q}_i \quad (2.38)$$

\bar{q}_i is the normalized charge for each particle given by

$$\bar{q}_i = \frac{\Delta t^2}{\Delta V} \frac{q_0}{m_0} q_i \quad (2.39)$$

where $\Delta V = \text{tr}(\Delta \mathbf{r})$.

2.3.6 Solver

Due to normalization already inherent in the charge distribution, $\bar{\rho}_j$, and in the application of the electric field, $\bar{\mathbf{E}}$, to each particle the solver can disregard the normalization.

2.4 Grid Structs and Partitioning

In this section our overall parallelization strategy is discussed as well as the storage needs for the grids.

2.4.1 Data structures

The fields and quantities in our PiC model is discretized on a threedimensional grid and comes to use several places in the method. In the multigrid calculation we also have a use for several grids of varying spatial coarseness. So it will be useful for us to organize the data so that we have the grid stored as an independent structure available for the program, while the multigrid part uses an extended version where it also has access to the different subgrids of different coarseness. Each multigrid struct will have an array of different subgrids, where the first is a pointer to the fine grid used in the rest of the calculations, this makes it easy to select a grid level to perform an algorithm on.

2.4.2 Domain partitioning

We have chosen to divide the physical domain onto the different processors that each take care of a physical subdomain. This is known as Domain Partitioning, and suits our distribution algorithm as well as the multigrid method, see section 2.7.1 for the consequences of Domain Partitioning for multigrids. Since each subdomain only needs to store the particles, and grids, on its physical subdomain the model can be upscaled in principle without any additional need for memory storage, by adding more processors. The subdomains are dependent on each other and we need some communication between them, which we solve by letting each subdomain also store the edge of the neighboring subdomain. Depending on the boundary conditions it could also be useful to store an extra set of values on the outer domain boundary as well, which will be called ghost points, N_G . The extra grid points due the the overlap between the subdomains we will call overlap points, N_O . Let us for simplicity sake consider a regular domain, with equal extent in all dimensions, with N grid points per dimension, d and consider how many grid values we need to store as a singular domain and the grid values needed when it is divided amongst several processors, a 2 dimensional case is depicted in fig. 2.2.

2.4.3 Singular domain

In the case where the whole domain is worked on by one process we need N^d to store the values on the grid representing the physical problem, in addition we see that we also need to store values for the ghost points along the domain boundary. Given that we have one layer of ghost points on all the boundaries,

and there is 2 boundaries per dimension, the total number of ghost points is given by $N_G = 2dN$. Since there is only 1 domain we don't need to account for any overlap between subdomains and the total grid points we need to store is:

$$N_{Tot} = N^d + N_G + N_O = N^d + 2dN^{d-1} \quad (2.40)$$

For the 2 dimensional case, in fig. 2.2, that adds up to $N_{Tot} = 8^2 + 2 \times 4 \times 8 = 128$.

2.4.4 Several subdomains

In the case where we introduce several subdomain, in addition to storing the grid values and the ghost points we also need to store an overlap between the subdomains. If we take our whole domain Ω and divide it up into several small domains Ω_S , the smaller domains only takes a subsection of the grid points. For simplicity case, and equal load on processors, we let the subdomains as well be regular, with the whole domain being a multiple of the subdomains. Our whole domain has N grid points in each direction, if we then divide that domain into $\#\Omega$ domains, then each of those subdomains will have $N_S = N^d / \#\Omega$ grid points. Each of those subdomains will also need values representing the ghost points and overlap from the neighboring nodes. A boundary of a subdomain will either have overlap points, or ghost points, not both at the same time so for each boundary we need to 1 layer, N_S^{d-1} . Each subdomain will have 2 boundaries per dimension since we have regular subdomains. The total number of grid points needed per subdomain is then

$$N_{Tot,S} = N_S^d + (N_G + N_O) = N_S^d + 2dN_S^{d-1} \quad (2.41)$$

while the total number of grid points is

$$N_{Tot} = \#\Omega N_{Tot,S} \quad (2.42)$$

For the 2 dimensional case discussed earlier we need $N_{Tot,S} = 4^2 + 2 \times 2 \times 4^1 = 32$.

Since the effect of the subdomain boundaries increase the coarser the grid is we should not let the coarsest multigrid level be too small. We also don't need the spatial extent of the grid to be equal on all sides, but it was done here to keep the computations simple.

2.5 Multigrid - Expanded

Here I will go through the main theory and algorithm behind a multigrid solver, developed as a part of this thesis, as explained in more detail in (Press et al.,

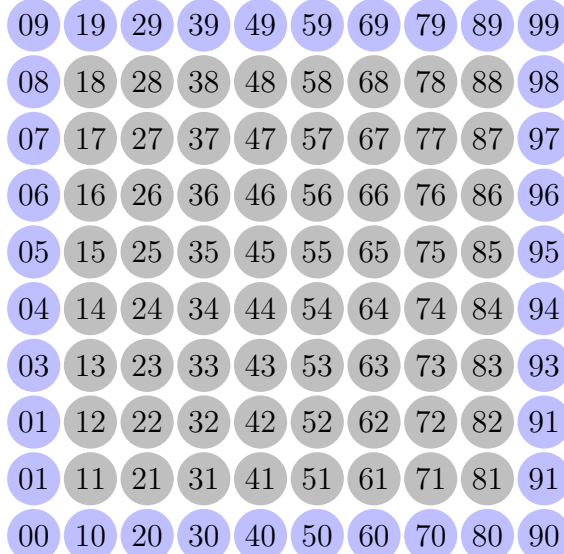
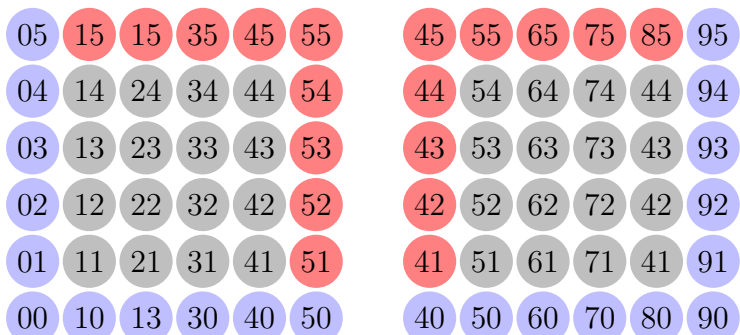
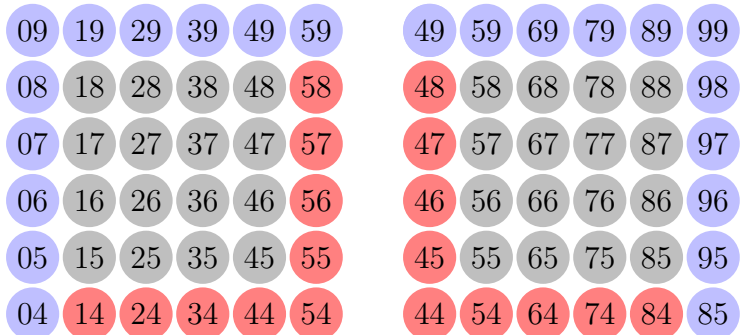
(a) The grid points needed for an 8×8 domain.(b) The 8×8 grid divided into 4 subdomains

Figure 2.2: Each circle in the figures represents 1 grid point, and the first number is the column while the second is the row. The grey colour represents physical space the computational node works on, the blue color is the outer grid points for boundary conditions and the red colour is the overlapping grid points.

1988; Trottenberg et al., 2000). This solver is developed with a wholly distributed storage model.

2.5.1 Algorithm

We want to solve a linear elliptic problem,

$$\mathcal{L}u = f \quad (2.43)$$

where \mathcal{L} is a linear operator, u is the solution and f is a source term. In our specific case the operator is given by the laplacian, the source term is given by the charge density and we solve for the electric potential.

We discretize the equation onto a grid of size q .

$$\mathcal{L}_q u_q = f_q \quad (2.44)$$

Let the error, v_q be the difference between the exact solution and an approximate solution to the difference equation (2.44), $v_q = u_q - \tilde{u}_q$. Then we define the residual as what is left after using the approximate solution in the equation.

$$d_q = \mathcal{L}_q \tilde{u}_q - f_q \quad (2.45)$$

Since \mathcal{L} is a linear operator the error satisfies the following relation

$$\mathcal{L}_q v_q = \mathcal{L}(u_q - \tilde{u}_q) + (f_q - f_q) \quad (2.46)$$

$$\mathcal{L}_q v_q = -d_q \quad (2.47)$$

The system can then be solved directly on this level with a chosen discretization. If we then increase the resolution to obtain a better solution, the system becomes exponentially harder to solve. The multigrid method approaches this problem by solving it on several different discretizations levels. We set up a systems of nested coarser regular grids, $\mathfrak{T}_0 \supset \mathfrak{T}_1 \supset \dots \supset \mathfrak{T}_\ell$, where 0 is the finest and ℓ is the coarsest grid. Then an iterative solver, which has the property of quickly converging of high frequency errors, i.e. local errors, is used on the finest grid. The remaining error is then transferred to a coarser grid where lower frequency errors are more easily found. The errors found on the coarser levels is then transferred up to the finest level as a correction. To transfer between the discretization coarseness we use restriction, \mathcal{R} , and prolongation, \mathcal{P} , operators. Due to the fewer grid points the problem is faster to solve on the coarser grid levels than on the fine grid. Applying the restriction and prolongation operators on the grid changes gives us the same grid discretized on a different level.

$$\mathcal{R}d_q = d_{q+1} \quad \text{and} \quad \mathcal{P}d_q = d_{q-1} \quad (2.48)$$

fig. 2.3 shows a schematic overview of a 3-level version of a multigrid V cycle. The needed operations on each level is described in greater detail in section 4.1.

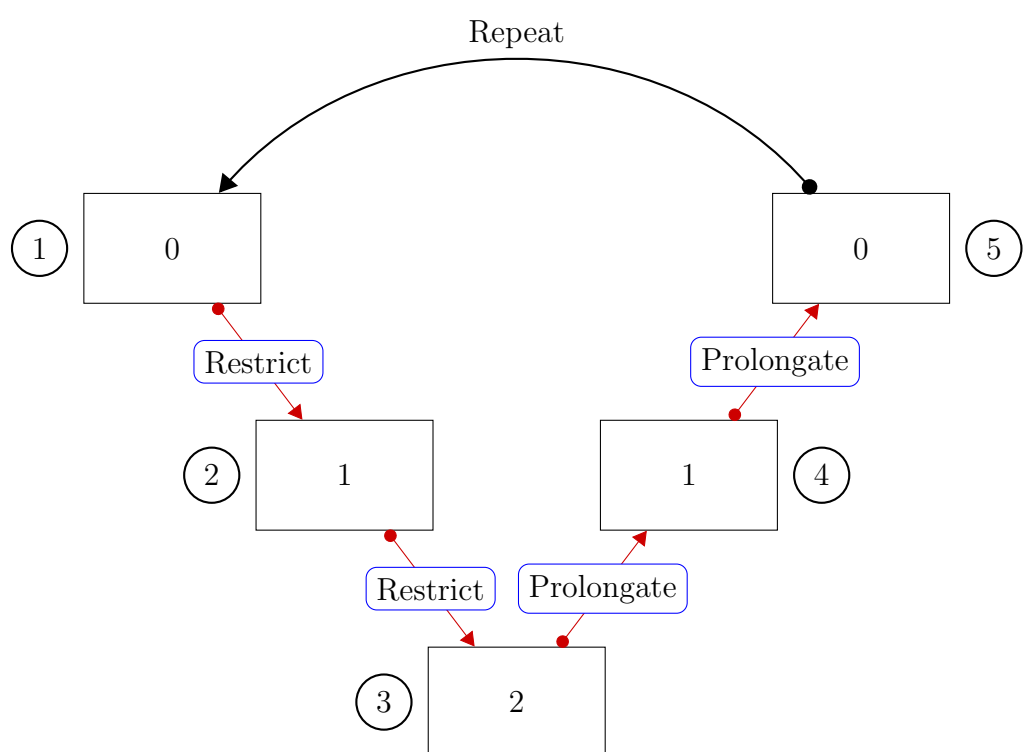


Figure 2.3: Schematic overview of the Multigrid cycle. In a three level MG implementation, there is 5 main steps in a cycle that needs to be considered.

V Cycle

TBD

W Cycle

TBD

FMG

TBD

2.5.2 Smoothing

(NOTE TO SELF: Mention 'chebyshev' polynomial as smoothing! And 'Lim' See zhukov) The multigrid method want iterative solvers as smoothers converges fast for the high frequency errors. The low frequency convergence, i.e. the long range interaction, is improved by lso solving it with coarser discretization. In this project we also wanted smoothers with good parallel scaling properties. We arrived at using Gauss-Seidel with Red and Black ordering. We ended with 1st order discretization of the Laplacian operator, as a compromise between simplicity in the program and the computational efficiency of hardcoded parts of the algorithms dealing with the Halo, i.e. ghost layers. It may be that higher order discretizations will yield better convergence and the project has some plans to expand to incorporate it.

Relaxation methods, such as Gauss-Seidel, work by looking for the setting up the equation as a diffusion equation, and then solve for the equilibrium solution.

So suppose we want to solve the elliptic equation

$$\mathcal{L}u = \rho \quad (2.49)$$

Then we set it up as a diffusion equation

$$\frac{\partial u}{\partial t} = \mathcal{L}u - \rho \quad (2.50)$$

By starting with an initial guess for what u could be the equation will relax into the equilibrium solution $\mathcal{L}u = \rho$. By using a Forward-Time-Centered-Space scheme to discretize, along with the largest stable timestep $\Delta t = \Delta^2/(2 \cdot d)$, we arrive at Jacobi's method, which is an averaging of the neighbors in addition to a contribution from the source term. By using the already updated values for the calculation of the u^{new} we arrive at the method called Gauss-Seidel which for two dimensions is the following

$$u_{i,j}^{n+1} = \frac{1}{4} (u_{i+1,j}^n + u_{i-1,j}^{n+1} + u_{i,j+1}^n + u_{i,j-1}^{n+1}) - \frac{\Delta^2 \rho_{i,j}}{4} \quad (2.51)$$

A slight improvement of the Gauss-Seidel algorithm is achieved by updating every other grid point at a time, by using Red and Black Ordering. This allows a vectorization of the problem and avoids any unnecessary copying.

Jacobian and Gauss-Seidel RB

The main iterative PDE solver, in this version of the multigrid program, is a Gauss-Seidel Red-Black, in addition a Jacobian solver was developed as a stepping stone and for testing purposes. It is a modification of the Jacobian method, where the updated values are used where available, which lead to it converging twice as fast (Press et al., 1988).

Our problem is given by $\nabla^2\phi = -\rho$, one way to think of the Jacobian method is as a diffusion problem, and with the equilibrium solution as our wanted solution. If we then discretize the diffusion problem by a Forward-Time-Centralized-Space scheme, we arrive at the Jacobian method, which is shown explicitly below for 1 dimension.

$$\frac{\partial \phi}{\partial t} = \nabla^2\phi + \rho \quad (2.52)$$

The subscript j indicates the spatial coordinate, and the superscript n is the 'temporal' component.

$$\frac{\phi_j^{n+1} - \phi_j^n}{\Delta t} = \frac{\phi_{j+1}^n - 2\phi_j^n + \phi_{j-1}^n}{\Delta x^2} + \rho_j \quad (2.53)$$

This is numerically stable if $\Delta t/\Delta x^2 \leq 1/2$, so using the timestep $\Delta t = \Delta x^2/2$ we get

$$\phi_j^{n+1} = \phi_j^n + \frac{1}{2} (\phi_{j+1}^n - 2\phi_j^n + \phi_{j-1}^n) + \frac{\Delta x^2}{2} \rho_j \quad (2.54)$$

Then we arrive at the Jacobian method

$$\phi_j^{n+1} = \frac{1}{2} (\phi_{j+1}^n + \phi_{j-1}^n + \Delta x^2 \rho_j) \quad (2.55)$$

The Gauss-Seidel method uses updated values, where available, and is given by

$$\phi_j^{n+1} = \frac{1}{2} (\phi_{j+1}^n + \phi_{j-1}^{n+1} + \Delta x^2 \rho_j) \quad (2.56)$$

Following the same procedure we get the Gauss-Seidel method for 2 and 3 dimensions.

$$\phi_{j,k}^{n+1} = \frac{1}{4} (\phi_{j+1,k}^n + \phi_{j-1,k}^{n+1} + \phi_{j,k+1}^n + \phi_{j,k-1}^{n+1} + \Delta x^2 \rho_{j,k}) \quad (2.57)$$

$$\phi_{j,k,l}^{n+1} = \frac{1}{8} (\phi_{j+1,k,l}^n + \phi_{j-1,k,l}^{n+1} + \phi_{j,k+1,l}^n + \phi_{j,k-1,l}^{n+1} + \phi_{j,k,l+1}^n + \phi_{j,k,l-1}^{n+1} + \Delta x^2 \rho_{j,k,l}) \quad (2.58)$$

Here we have implemented a different version of the Gauss-Seidel algorithm called Red and Black ordering, which has conceptual similarities to the leapfrog algorithm, where usually position and velocity is computed at t and $t + (\delta t)/2$. Every other grid point is labeled a red point, and the remaining is black. When updating a red node only black nodes are used, and when updating black nodes only red nodes are used. Then a whole cycle consists of two halfsteps which calculates the red and black nodes seperately.

- For all red points:

$$\phi_{j,k,l}^{n+1/2} = \frac{1}{8} (\phi_{j+1,k,l}^n + \phi_{j-1,k,l}^n + \phi_{j,k+1,l}^n + \phi_{j,k-1,l}^n + \phi_{j,k,l+1}^n + \phi_{j,k,l-1}^n + \Delta x^2 \rho_{j,k,l})$$

- For all black points:

$$\phi_{j,k,l}^{n+1} = \frac{1}{8} (\phi_{j+1,k,l}^{n+1/2} + \phi_{j-1,k,l}^{n+1/2} + \phi_{j,k+1,l}^{n+1/2} + \phi_{j,k-1,l}^{n+1/2} + \phi_{j,k,l+1}^{n+1/2} + \phi_{j,k,l-1}^{n+1/2} + \Delta x^2 \rho_{j,k,l})$$

2.5.3 Restriction

The multigrid method (MG) has several grids of different resolution, and we need to convert the problem between the diffrent grids during the overarching the MG-algorithm. The restriction algorithm has the task of translating from a fine grid to a coarser grid. Direct insertion is the simplest way to do this, where coarse grid points corresponds directly to its representation on the fine grid. In this implementation we chose to use a half weight stencil, which works well together with the 1 layer Halo, to restrict a quantity from a fine grid to a coarse grid. A higher order restriction algorithm could later be implemented if thought useful. The coarse grid values is obtained by giving half weighting to the fine grid point corresponding directly to the coarse grid point, and gives the remaining half to the adjacent fine grid values, see (2.59), for 1D, 2D and 3D examples.

$$\begin{aligned} \mathcal{R}_{1D} &= \frac{1}{4} [1 \ 2 \ 1] \\ \mathcal{R}_{2D} &= \frac{1}{8} \begin{bmatrix} 0 & 1 & 0 \\ 1 & 4 & 1 \\ 0 & 1 & 0 \end{bmatrix} \\ \mathcal{R}_{3D} &= \frac{1}{12} \left(\begin{bmatrix} 0 & 0 & 0 \\ 0 & 1 & 0 \\ 0 & 0 & 0 \end{bmatrix}, \begin{bmatrix} 0 & 1 & 0 \\ 1 & 6 & 1 \\ 0 & 1 & 0 \end{bmatrix}, \begin{bmatrix} 0 & 0 & 0 \\ 0 & 1 & 0 \\ 0 & 0 & 0 \end{bmatrix} \right) \end{aligned} \quad (2.59)$$

2.5.4 Prolongation

Along with the restriction operator described in the previous section, we also need prolongation operator to go from a coarse grid to a finer grid. As in the restriction operator direct insertion is the simplest algorithm. Here we will use bilinear interpolation, as advised in Trottenberg et al., 2000, for two dimensions and trilinear interpolation for 3 dimensions. In bilinear interpolation separate linear interpolation is done in the x- y- and z-direction, then those are combined to give a result on the wanted spot. (Note to self: Add source here) The same concept is expanded to give trilinear interpolation. The two and three dimensional stencils is given in (2.60)

$$\begin{aligned}\mathcal{P}_{2D} &= \frac{1}{4} \begin{bmatrix} 1 & 2 & 1 \\ 2 & 4 & 2 \\ 1 & 2 & 1 \end{bmatrix} \\ \mathcal{P}_{3D} &= \frac{1}{8} \left(\begin{bmatrix} 1 & 2 & 1 \\ 2 & 4 & 2 \\ 1 & 2 & 1 \end{bmatrix}, \begin{bmatrix} 2 & 4 & 2 \\ 4 & 8 & 4 \\ 2 & 4 & 2 \end{bmatrix}, \begin{bmatrix} 2 & 2 & 1 \\ 2 & 4 & 2 \\ 1 & 2 & 1 \end{bmatrix} \right)\end{aligned}\tag{2.60}$$

2.6 Boundary conditions

A simulation must necessarily have finite extent, we need to employ boundary conditions to deal with the edges of the simulation. Here we will go through 3 different schemes corresponding to periodic boundaries, depicted in fig. 2.4, Dirichlet conditions and Von Neumann conditions. Periodic conditions is used when we want to simulate an infinite plasma sheet. It is fitting to use when the plasma sheet is of a much larger extent than the length scale of the phenomena we want to investigate, or when we the investigated dynamics happen away from the edges. Dirichlet conditions is useful when the voltage on the edge of the simulation can be known beforehand, as it is often in laboratory experiments. When the electric field, or alternatively gradient of the voltage, along the edges is known von Neumann conditions should be used. The boundary conditions must also be coupled with fitting boundary conditions applied to the particles in a full PiC simulation. Particle conditions include periodic, bouncing and absorbing boundaries. To maintain the design aim of inherent modularity of our PiC model, the boundary conditions are defined using ghost points, avoiding different discretization stencils at the boundary. This reduces the complexity the smoothers, makes the boundary conditions easier to implement and opens the possibility of using them with other solvers.



(a) A 1 dimensional domain with grid points before the boundary conditions has been applied. The numbers denote the indexes for the values in the grid array. The blue grid points, (1 – 7) represents the true grid and the grey points, (0 and 8), is the ghost cell values. The concepts illustrated here should easily be expanded to more dimensions.



(b) Here periodic boundary conditions has been applied to the 1D domain above. Here and in the following the red color means a point has been changed. The ghost points at the edges has been set to equal the true grid points at the opposite edge giving periodic boundary conditions.



(c) For Dirichlet boundary conditions we have predetermined values along the edge, this are here represented as the ghost cells being set to a given value defined by $\partial\Omega_i$. The boundary function can be as simple as setting everything along the edge to a constant, but it could also be a spatially and time varying function. It is also possible to let it correspond to input given by coupled computer model.



(d) Von Neumann boundary conditions specifies what the derivative is on the edge. To achieve that we set the ghost points to a specified value that will give the wanted derivative when a finite difference method swipes over the point. For the left side the function should be set to $f_0 = u_2 - 2\Delta x A$ and to $f_8 = u_6 - 2\Delta x A$ for the right side. Here A is the predetermined values that the derivative should correspond to.

Figure 2.4: An overview of 3 boundary conditions applied to a 1D domain.

2.6.1 Periodic Boundaries

With periodic boundary conditions we want the boundary on one side to be equal to the field on the other side of the plasma. For the 1D case, see fig. 2.4b, this can be written as

$$\nabla^2 \phi = -\rho \quad \Omega = [0, L] \quad (2.61)$$

With boundaries

$$\phi(0) = \phi(L) \quad (2.62)$$

Here we should note that this is very similar to what happens between the subdomains in a Domain Partitioning parallelization scheme, so often the same algorithm and code can be reused to achieve periodic boundary conditions.

Solutions for the continuous problem with periodic boundary conditions exists only if the *compatibility condition* (Trottenberg et al., 2000)

$$\int_{\Omega} \rho d\mathbf{x} = 0 \quad (2.63)$$

is held. This means that the total charge in the domain must be zero, which is often true in plasma due to quasi-neutrality.

To ensure a unique discretized solution need to set the integration constant, this can be done by setting a *global constraint* on the solution

$$\sum_{\Omega} \phi = 0 \quad (2.64)$$

2.6.2 Dirichlet Boundaries

With Dirichlet conditions the boundaries of the potential are known and given by a function, $\partial\phi = f$. Then a 1D problem, fig. 2.4c, is represented by

$$\nabla^2 \phi = -\rho \quad \Omega = [0, L] \quad (2.65)$$

with boundaries

$$\phi(0) = f(0), \quad f(L) = f(L) \quad (2.66)$$

2.6.3 Neumann Boundaries

Now we assume we know the gradient of the potential along the boundary, $\nabla\phi_{\partial\Omega} = f$. This is often used in hydrodynamics to represent reflecting boundaries. Then our 1D example problem will look like

$$\nabla^2 \phi = -\rho \quad \Omega = [0, L] \quad (2.67)$$

with boundaries

$$\partial\phi(0) = f(0), \quad \partial\phi(L) = f(L) \quad (2.68)$$

The boundary condition is then stated as a gradient and we need to approximate it to ϕ to use it in the poisson equation, eq. (2.67). We do this by a 2nd order central difference to the gradient.

$$\frac{\partial\phi(x)}{\partial x} = \frac{\phi(x + \Delta x) - \phi(x - \Delta x)}{2\Delta x} = f(x) \quad (2.69)$$

At the lower boundary, $x = 0$, this can then be written as

$$\phi(-\Delta x) = \phi(\Delta x) - 2\Delta x f(0) \quad (2.70)$$

and at the upper

$$\phi(L + \Delta x) = \phi(L - \Delta x) - 2\Delta x f(L) \quad (2.71)$$

With our discretization, where the internal cell sizes are 1, the $\phi(-\Delta x)$ correspond directly to a ghost cell. So we can implement the Neumann boundary conditions easily by setting the ghost cells equal to eqs. (2.70) and (2.71), see fig. 2.4d. This scheme completely avoids any modification of the smoother stencils at the boundaries.

2.6.4 Boundaries in Multigrid

The multigrid algorithm solves the problem on several discretization levels. Due to this we need to represent the boundaries on the coarser grid levels as well.

Periodic

Since the periodic boundary conditions can be tough of to set the domain next a copy of itself the boundary treatment will remain equal on the coarser grids. It should also be mentioned that the *global constraint*, eq. (2.64), only needs to be set on the coarsest grids to achieve good convergence rates (Trottenberg et al., 2000).

Dirichlet

The Dirichlet condition specifies the potential at the boundaries. Since the conditions should apply to the problem at all coarseness levels, we need a restriction operator specific to the boundary.

The easiest boundary restriction operator is direct injection, letting each coarse grid point correspond to a grid point on the boundary of the finer grid. This is often sufficient, especially in the case of spatially constant boundaries. If the boundaries constant in time computing time can be saved by computing the boundaries for all levels once at the start of the simulation.

If the boundaries are more complicated first or second order interpolation could be used to restrict them.

Neumann

The Neumann conditions are dependent on the next to outermost grid point, i.e. grid point 2 in fig. 2.4d on the lower side, because of this they will have to be recomputed each time they are used. But still the function f should be restricted separately from the finer grid restriction.

2.6.5 Mixed Conditions

All the boundary conditions can be implemented with the use of ghost cells, this enables the use of the 5-point stencil for the smoothers. This greatly simplifies mixed boundary conditions, the boundaries are set on the ghost layer of the grid separately, then the smoother runs. Here it should be noted that the boundaries need to be reset for each halfcycle in GS-RB.

As can be seen in fig. 2.5 we do not have to care for the corners of the domain, as long as we are using a 5-point stencil. This allows us to not need to care of which boundary conditions takes precedence when they clash. For a higher order, or different, stencils the corner ghost cells may be important and the mixing of boundary conditions need to be given extra care.

2.7 Parallelization

For the parallelization of an algorithm there are two obvious issues that need to be addressed to ensure that the algorithm retains a high degree of parallelization; communication overhead and load imbalance (Hackbusch and Trottenberg, 1982). Communication overhead means the time the computational nodes spend communicating with each other, if that is longer than the actual time spent computing the speed of the algorithm will suffer, and load imbalance appears if some nodes need to do more work than others causing some nodes to stand idle.

Here we will focus on multigrid of a 3D cubic grid, where each grid level has half the number of grid points. We will use grid partitioning to divide the domain, GS-RB (Gauss-Seidel Red-Black) as both a smoother and a coarse grid solver.

We need to investigate how the different steps: interpolation, restriction, smoothing and the coarse grid solver, in a MG algorithm will handle parallelization.

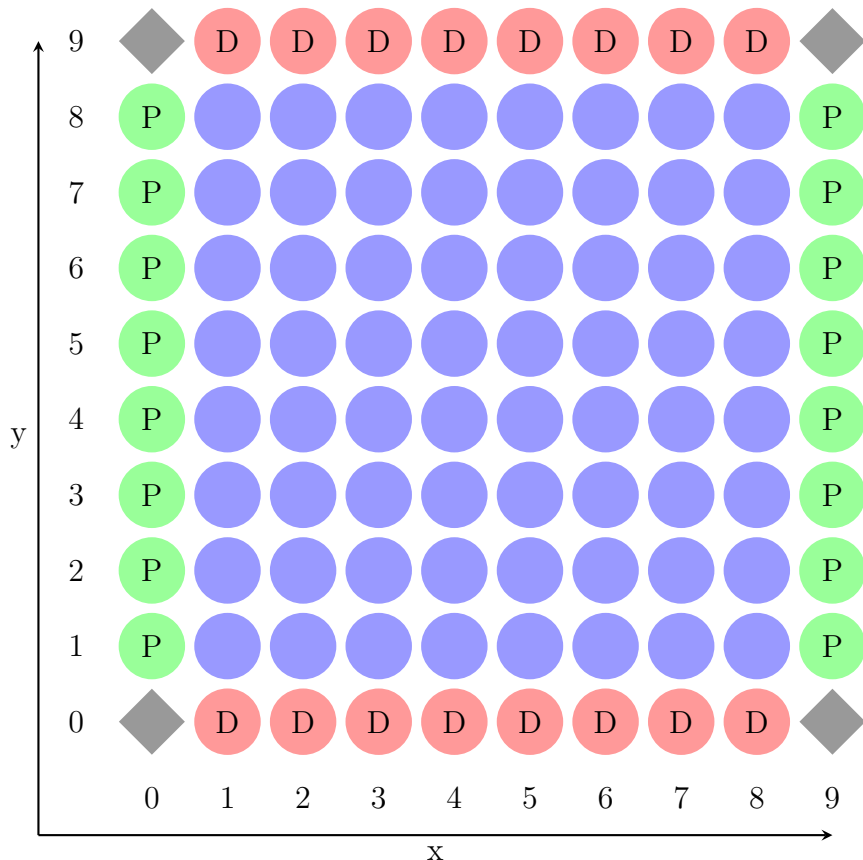


Figure 2.5: This is a 2D domain with mixed boundary conditions, along the x -axis there are periodic boundary conditions, green ghost points, and the y -axis there are dirichlet boundary conditions, red ghost points. If the smoothers are using a 5 point discretization stencil the corners, grey diamonds, are neglected when computing the inner, i.e. true, grid.

2.7.1 Grid Partition

There are several well explored options for how a multigrid method can be parallelized, for example Domain Decomposition (Arraras et al., 2015) (fix accent), Algebraic Multigrid (Stüben, 2001), see Chow et al. (2006) for a survey of different techniques. Here we will focus on Geometric Multigrid (GMG) with domain decomposition used for the parallelization, as described in the books Trottenberg et al., 2000; Hackbusch and Trottenberg, 1982.

With domain partitioning we divide the grid \mathcal{T} into geometric subgrids, then we can let each processes handle one subgrid each. As we will see it can be useful when using the GS-RB smoothing, as well as other parts of a PiC program, to extend the subgrids with layers of ghost cells. The GS-RB algorithm will directly need the adjacent nodes, in its neighbour subdomain.

2.7.2 Distributed and accumulated data

One possible strategy to implement a parallel multigrid solver is to keep some of the quantities distributed, ie, they are only stored locally on the local computational nodes, while the other are accumulated and shared between the nodes. Below follows an overview of which quantities needs only be accessed locally and which needs a global presence during a parallel execution of the code. (Where did I read this again??)

- u solution (Φ)
- w temporary correction
- d defect
- f source term (ρ)
- \mathcal{L} differential operator
- \mathcal{P} prolongation operator
- \mathcal{R} restriction operator
- **\mathbf{u}** Bold means accumulated vector
- $\tilde{\mathbf{u}}$ is the temporary smoothed solution
- Accumulated quantities: $\mathbf{u}_q, \hat{\mathbf{u}}_q, \tilde{\mathbf{u}}_q, \hat{\mathbf{w}}_q, \mathbf{w}_{q-1}, \mathcal{P}, \mathcal{R}$
- Distributed quantities: f_q, d_q, d_{q-1}

To avoid the accumulated quantities, which can cause memory issues, we have instead gone for a strategy where all the quantities are only locally distributed. Instead of gathering the all of the accumulated quantities, each of the subdomains gathers only the needed part of the quantities from its neighboring subdomains. With this strategy the local memory needs should not increase as the number of processors grow.

2.7.3 Smoothing

We have earlier divided the grid into subgrids, with overlap, as described in subsection 2.7.1 and given each processor responsibility for a subgrid. We broadly follow the algorithm in Adams, 2001. A GS-RB algorithm start with a guess, or approximation, of the solution $u_{i,j}^n$. Then we will obtain the next iteration by the following formula, for a 2D case,

$$u_{i,j}^{n+1} = \frac{1}{4} (u_{i+1,j}^n + u_{i-1,j}^n + u_{i,j+1}^n + u_{i,j-1}^n) - \frac{\Delta^2 \rho_{i,j}}{4} \quad (2.72)$$

We can see that for the inner subgrid we will have no problems since all the surrounding grid points are known. On the edges we will need the adjacent grid points that are kept in the other processors. To avoid the algorithm from asking neighboring subgrids for adjacent grid points each time it reaches a edge we instead update the entire neighboring column at the start. So we will have a 1-row overlap between the subgrids, that need to be updated for each iteration.

2.7.4 Restriction

For the transfer down a grid level, to the coarser grid we will use a half weighting stencil. In two dimensions it will be the following

$$\mathcal{R} = \frac{1}{8} \begin{bmatrix} 0 & 1 & 0 \\ 1 & 4 & 1 \\ 0 & 1 & 0 \end{bmatrix} \quad (2.73)$$

With the overlap of the subgrids we will have the necessary information to perform the restriction without needing communication between the processors (Hackbusch and Trottenberg, 1982).

2.7.5 Interpolation

For the interpolation we will use a bilinear, or trilinear, interpolation stencil, which for 2 dimensions is:

$$\mathcal{P} = \frac{1}{4} \begin{bmatrix} 1 & 2 & 1 \\ 2 & 4 & 2 \\ 1 & 2 & 1 \end{bmatrix} \quad (2.74)$$

Since the interpolation is always done after GS-RB iterations the the outer part overlapped part of the grid updated, and we can have all the necessary information.

2.7.6 Scaling

Volume-Boundary effect

While a sequential MG algorithm has a theoretical scaling of $\mathcal{O}(N)$ (Press et al., 1988), where N is the number of grid points, an implementation will have a lower scaling efficiency due to interprocessor communication. We want a parallel algorithm that attains a high speedup with more added processors P , compared to sequential 1 processor algorithm. Let $T(P)$ be the computational time needed for solving the problem on P processors. Then we define the speedup $S(P)$ and the parallel efficiency $E(P)$ as

$$S(P) = \frac{T(1)}{T(P)} \quad E(P) = \frac{S(P)}{P} \quad (2.75)$$

A perfect parallel algorithm would the computational time would scale inversely with the number of processors, $T(P) \propto 1/P$ leading to $E(P) = 1$. Due to the necessary interprocessor communication that is generally not achievable. The computational time of the algorithm is also important, if the algorithm is very slow but has good parallel efficiency it is often worse than a fast algorithm with a worse parallel efficiency.

The parallel efficiency of an algorithm is governed by the ratio between the time of communication and computation, T_{comm}/T_{comp} . If there is no need for communication, like on 1 processor, the algorithm is perfectly parallel efficient. In our case the whole grid is diveded into several subgrids, which is assigned to different processors. In many cases the time used for computation is roughly scaling with the interior grid points, while the communication time is scaling with the boundaries of the subgrids. If a local solution method is used on a local problem it is only the grid points at the boundary that needs the information from grid points on the other processors. Since the edges has lower dimensionality than the inner grid points it the inner domain outgrows the edges. As the size of the subdomains is increasing the computational time increases faster than the time for communication. This causes a parallel algorithm to often have higher parallel efficiency on a larger problem. This is called the Boundary-Volume effect.

	Cycle	Sequential	Parallel
MG	V	$\mathcal{O}(N)$	$\mathcal{O}(\log N)$
	W	$\mathcal{O}(N)$	$\mathcal{O}(\sqrt{N})$
FMG	V	$\mathcal{O}(N)$	$\mathcal{O}(\log^2 N)$
	W	$\mathcal{O}(N)$	$\mathcal{O}(\sqrt{N} \log N)$

Table 2.1: The parallel complexities of sequential and parallel multigrid cycles. (NOTE TO SELF: See also Zhukov et al., 2014)

Parallel complexity

The complexities, as in needed computational work, of sequential and parallel MG cycles is calculated in Hackbusch and Trottenberg, 1982 and is shown in table 2.1. In the table we can see that in the parallel case there is a substantial increase in the complexity in the case of W cycles compared to V cycles. In the sequential case the change in complexity when going to a W cycle is not dependent on the problem size, but it is in the parallel case.

Chapter 3

Implementation

3.1 General idea

An iterative solver solves a problem by starting with an initial guess, then it performs an algorithm improving the guess and repeats with the improved guess. The difference between the guess and the correct solution, the residual, does not necessarily converge equally fast for different frequencies. An iterative solver can be very efficient on reducing the local error, while the errors due to distant influence is reduced slowly. A multigrid solver attacks this problem by applying iterative methods on different discretizations of the problem, by solving on a very coarse grids the error due to distant influence will be reduced faster, while solving on a fine grid reduces the local error fast. So by solving on both fine and coarse grids the needed cycles will be reduced. To implement a multigrid algorithm we then need algorithms to solve the problem on a grid section 2.5.2, restriction section 2.5.3 and prolongation section 2.5.4 operators to transfer the problem between grids, as well as a method to compute the residual.

3.1.1 V-cycle

The simplest multigrid cycle is called a V-cycle, which starts at the finest grid, goes down to the coarsest grid and then goes back up to the finest grid. First the problem is smoothed on the finest level, then we compute the residual, or the rest after inserting the guess solution in the equation. The residual is then used as the source term for the next level, and we restrict it down as the source term for the next coarser level and repeat until we reach the coarsest level. When we reach the coarsest level the problem is solved there and we obtain a correction term. The correction term is prolongated to the next finer level and added to the solution there, improving the solution, following by a new smoothing to obtain a new correction. This continues until we reach the finest level again and a multigrid cycle is completed, see fig. 2.3 for a 3 level schematic.

In the following description of the steps in the MG method, we will use ϕ , ρ , d and ω to signify the solution, source, defect and correction respectively. A subscript means the grid level, where 0 si the finest level, while the superscript 0 implies an initial guess is used. Hats and tildes are also used to signify the stage the solution is in, with a hat meaning the solution is smoothed and a tilde meaning the correction from the grid below is added.

The overarching algorithm is shown in algorithm 2

Algorithm 1 Multigrid V cycle

```

if level = coarsest then
    Solve           |  $\hat{\phi}_l = \mathcal{S}(\phi_l, \rho_l)$ 
    Interpolate correction |  $\omega_{l-1} = \mathcal{I}\phi_l$ 
else
    for each level do
        Smooth           |  $\hat{\phi}_l = \mathcal{S}(\phi_l, \rho_l)$ 
        Residual          |  $d_l = \nabla^2\hat{\phi}_l - \rho_l$ 
        Restrict           |  $\rho_{l+1} = \mathcal{R}d_l$ 
        Go down, recieve correction |  $\omega_l = \text{MG}(\phi_{l+1})$ 
        Add correction    |  $\tilde{\phi}_l = \hat{\phi}_l + \omega_l$ 
        Smooth           |  $\phi_l = \mathcal{S}(\tilde{\phi}_l, \rho_l)$ 
        Interpolate correction |  $\omega_{l-1} = \mathcal{I}\phi_l$ 

```

At the coarsest level the the problem is solved directly and the correction is propageted upward.

3.1.2 Updating the Halo

All of the subgrids has a halo of ghostslayers around it, which is used to simplify boundary conditions and subdomain communication. Each computational node represents a subdomain of the whole, with the neighboring node being the boundary. So between two subdomains each subdomain updates the boundary according to the neigbouring subdomain. In addition the halo is used to facilitate boundary conditions on the whole domain. For some of the grid operators the ghost are not used, while some of them need updated values. All of the iterative solvers, that are used for smoothing, need updated values of the of the solution, ϕ . The prolongation and residual operators need updated values for the solution ϕ , and the restrictor need updated residual values, ρ , as long as direct insertion is not used. (NOTE TO SELF: belong in paralellization part) We also need to take into account that the smoothers outputs an updated halo for ϕ , to avoid unnecessarily communication between the processors.

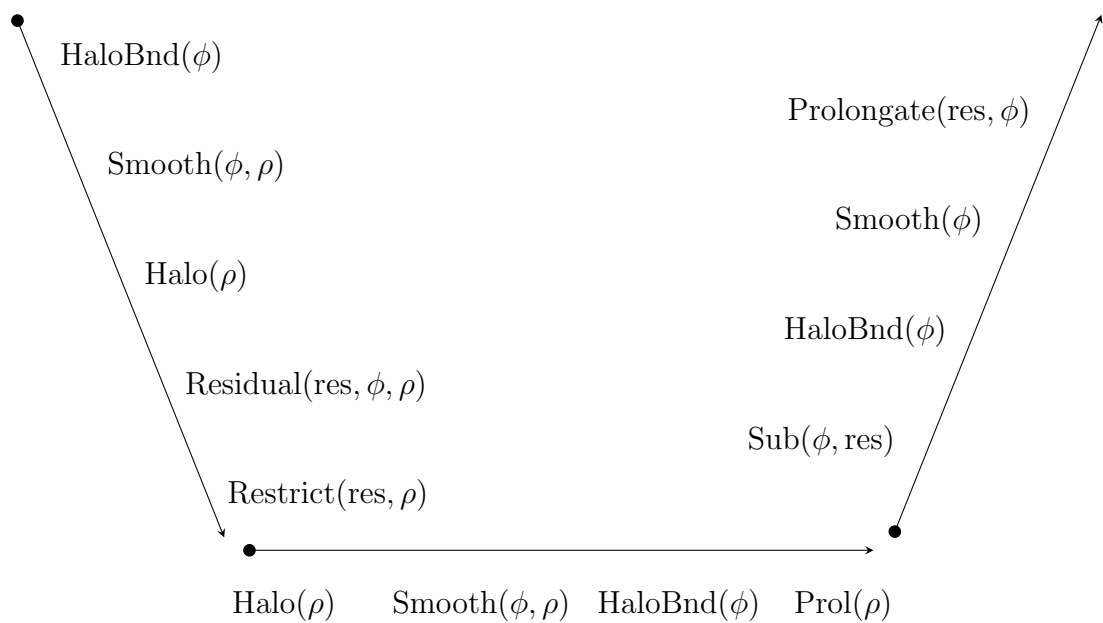


Figure 3.1: The functions used in 2 grid deep multigrid. The algorithm follows the

3.1.3 Implementation

In general there are 4 different quantities, the source, the solution, the residual and the correction, we need to keep track of. On each grid level the residual is computed, then it is set as the source term for the next level and then it is not used more. The correction, the improvement to the finer grid, is only used when going to a finer grid. Due to this we can save some memory by letting the correction and the residual share the same memory, so both are stored in the mgRes struct. There are a regular as well as a recursive implementation of a V-cycle. The functions takes the current level, the bottom of the cycle as well as the end point of the cycle. So several different cycles can be built from the functions. A W cycle can be built a V cycle that starts at the finest level and stops at a mid level, and then a new V-cycle is started at the mid level that ends at the finest level. A full multigrid algorithm (FMG) can also be implemented by first restricting the original source term down to the coarsest level and then run a V-cycle that ends at the finest level. (Note: there will be a a general mgSolver function pointer that can be set to prebuilt cycles, so the cycle can be set from the input file)

The regular V cycle algorithm is quite straightforward, first it restricts and computes itself down to the bottom level, then it solves it directly on the bottom level. Then the correction is brought up and improved through the grid up to the top level. See ?? for an example code.

The recursive algorithm uses an algorithm more similar to the one described in ?. First it computes the steps necessary so the grid below has an updated source term, then it calls itself on a lower level. After receiving the correction from the lower level it is improved and sent to the level above. If the function is at the bottom level, it solves the problem directly and sends the correction up. See ?? for an example code.

3.2 Restriction

In our implementation we first cycle through all of the true coarse grid points, then the two main tasks is to find the specific fine grid point corresponding to the specific coarse grid point, and finding the indexes of the fine grid points surrounding the grid point.

Since the value in both grids are stored in a first order lexicographical array, we should treat the grid points in the same fashion, so the values are stored close to each other in the array. The first dimension is treated first, then the next dimension is incremented followed by treating the first dimension again, then increment the next and so on. The fine grid has twice the resolution of the coarse grid, so for each time the coarse grid index is incremented, the fine grid index is incremented twice.

Along the x-axis each incrementation is the number of values stored in the grid, which for scalars is 1 (This is only used for scalars, so now the 1 is hardcoded, I will need to test if using `size[0]` instead affects speed), and 2 for the fine index. The fine index will in addition need to skip 1 row each time, each time the y-axis is incremented, due to the finer resolution and 1 layer each time the z-axis is incremented.

At the edges of the grid we have ghost layers, which have equal thickness for both the grids, so the coarse grid needs to increment over the ghost values, in the x-direction, each time y is incremented. When z is incremented the index need to skip over a row of ghost values. The fine index follows the same procedure as the coarse index when dealing with the ghost layers.

When correct fine grid index is found, corresponding to a coarse grid index, the stencil needs to be applied around that grid value. This is done by first calculating the index of the first coarse and find indexes and setting the correct indexes for the surrounding grid values, then the surrounding grid indexes can be incremented exactly as the fine grid index and they will keep their shape around the fine grid index. Since our indexes in x, y and z are labeled j,l,k, the next value along the x-axis is labeled 'fj' and the previous is labeled 'fjj'. The coarse and fine grid indexes are label 'c' and 'f' respectively.

3.3 Prolongation

The algorithm implemented for the interpolation is based on the method, described in Press et al., 1988, has the following steps, which is also shown for a 2D case in 4.2.

1. Direct insertion: Coarse→ Fine
2. Interpolation on highest Dimension: $f(x) = \frac{f(x+h)+f(x-h)}{2h}$
3. Fill needed ghosts.
4. Interpolation on next highest Dimension

The interpolation should always first be done on the highest dimension, because the grid values are stored further apart along the highest axis in the memory, and the each successive interpolation needs to apply to more grid points. (Note to self: should test)

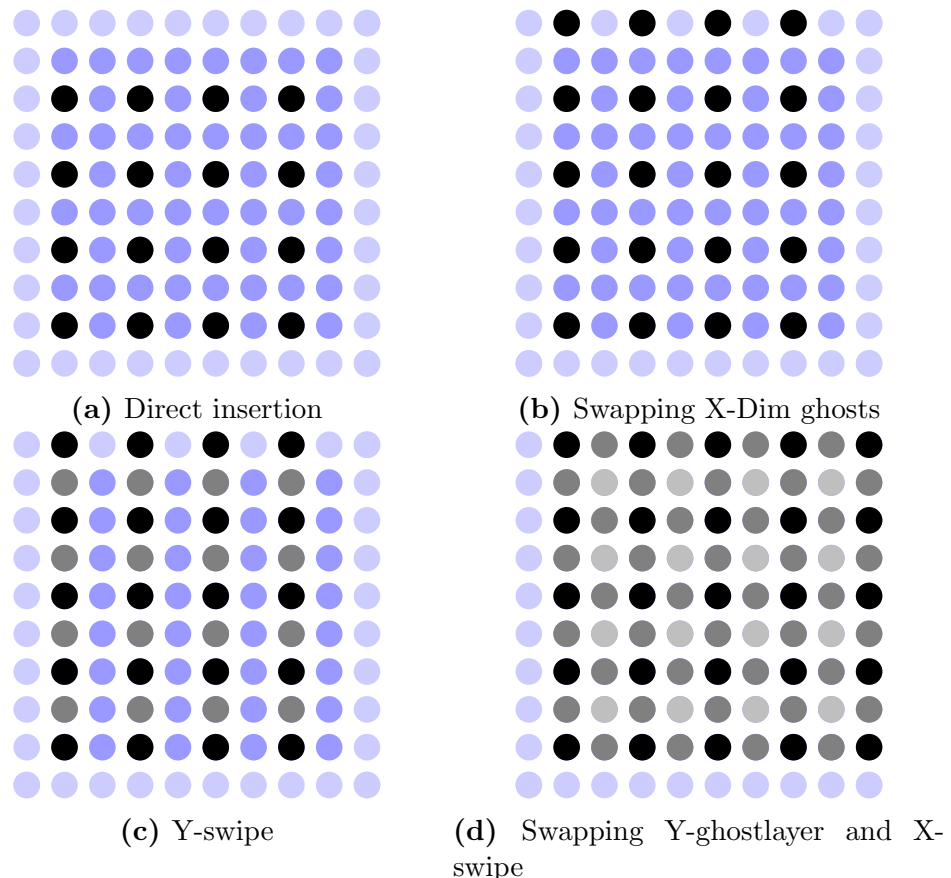


Figure 3.2: This figure shows the steps in computing the prolongation stencil in an $[8 \times 8]$ grid. First a direct insertion from the coarse grid is performed (4.2a), followed by filling the ghostlayer perpendicular to the x-axis from the neighbouring grid (4.2b). Then a swipe is performed in the y-direction filling the grid points between, taking half the value from the node above, and half from the node below (4.2c). Then a ghost swap is performed before doing a swap in the x-direction (4.2d).

3.4 Smoothers

Jacobi's method

The implementation of the jacobian algorithm is straightforward, but it has the downside of slow convergence and bad smoothing properties, in addition to needing an additional grid values. When ϕ_i^{n+1} is computed we need access to the previous value ϕ_{i-1}^n , and more values in higher dimensions, so either the previous values need to stored seperately, or ϕ_i^{n+1} can be computed on a new grid and then copied over after completing the cycle. In this implementation we computed on a temporary grid and then copied over, since it was mostly for debugging purposes and efficiency was not a concern.

The computation is done by starting at index $g = 0$, computing the surrounding grid indexes, gj, gjj, \dots , where gj is the next grid point along the x-axis, and gjj is the previous value. Then the entire grid is looped trough over, incrementing both g and the surrounding grid indexes gj, gjj, \dots . The computation on the ghost layers will be incorrect but those will be overwritten when swapping halos. See ?? for an example code in 2D.

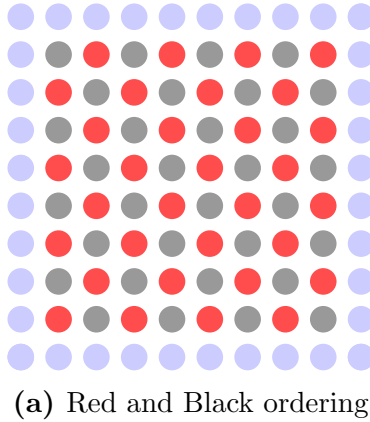
Gauss-Seidel Red and Black

In the implementation of Gauss-Seidel algorithm we use a clever ordering of the computations, called Red and Black ordering, both to increase the smoothing properties of the algorithm as well as avoiding creating a temporary grid to store ϕ^{n+1} in. Every grid point where the indexes sum up to an even number is labeled a red point and the odd index groupings are labeled black points, see fig. 4.3a. Then each red point is directly surrounded by only black points and vica versa.

A cycle is then divided into 2 halfcycles, where each halfcycle computes ϕ^{n+1} for the red and black points respectively.

1. for(int c = 0; c<nCycles; c++)
 - Cycle through red points and compute ϕ^{n+1}
 - Swap Halo
 - Cycle through black points and compute ϕ^{n+1}
 - Swap Halo

For the 2 dimensional case the cycling is done first for the odd rows and even rows seperately, due to the similarity between all the red points in the odd rows, and between the red points in the even rows. Then the cycling could be generalized into a static inline function used for all the cycling. See ?? for the 2D implementation.



(a) Red and Black ordering

For the 3 dimensional case there is now did two different takes on the problem, one where the iteration through the grid is streamlined, but needing several loops through the grid taking care of a subgroup of the grid points each loop. The other algorithm uses one loop through the grid, with different conditions on the edges to make it go through the correct grid points in each line.

When the loops are streamlined the edges the loop go through the entire grid, but when it reaches and edge in it either needs to add or subtract 1 to the iterator index. In we want to do a red pass, computing all the red values, the grid is cycled through increasing by 2 each time. Then it will access up the indexes, 36, 38, 40, 42, … . In the second row we want it to use the index 43, instead of 42, so we need to increase it by 1 when it reaches the edge. When it reaches the end of the second line, we want it to increase from 47 to 48, so then we need to subtract 1. In the next layer we need to shift the behaviour on the edges to the opposite. See

.
48	49	49	50	51	52
42	43	44	45	46	47
36	37	38	39	40	41

In the other implementation I tried something similar to the 2D implementation, where it does several loops through the grid, computing an easier subgroup of the red nodes each time, so the iteration index can increase by just to each time. So for the red points it computes the odd and even layers and rows seperately.

- Compute Odd layers, odd rows
- Compute Odd layers, even rows
- Compute Even Layers, odd rows
- Compute Even layers, even rows

3.5 Implementation of Boundary Conditions

Since the subdomains already need to exchange the halo, we already had made a suite of function dealing with halo-operations. These functions can get, set, add, etc. N-dimensional slices from the halo. As can be seen in ?? this is quite similar to the needs of the varying boundary conditions and we will reuse this capability during the implementation of boundary conditions. In addition we will also need methods to restrict the part of the conditions that need to be restricted. Here we will only deal with time-invariant boundary conditions so they can be set, and restricted, once during initializations of the grids. It should be easy to expand it to time varying conditions, just restrict the boundary function each timestep.

In general the condition types are stored as a 2Dim array, in the order $x_{low}, x_{upper}, y_{low}, \dots$. Each time the boundary conditions function is called it checks if each subdomain edge is at the total domain boundary. Since the outer subdomains need to do extra computations here, it shouldn't matter if the inner subdomains do some extra calculations. If the subdomain boundary is at the boundary it calls the a function depending on which boundary type the edge is.

3.5.1 Restriction

For now we have choosen to use straight injection, since we will not use any complicated boundary conditions in this project, other developers are welcome to expand it by more restriction algorithms.

3.5.2 Periodic

The periodic boundary conditions are just the same procedure as the halo exchange. To try too keep an even load, between the computational nodes, the halo exchange is also done between the the boundary subdomains.

To keep the convergence rate good we also need to keep the *global constraint* and *compatibility condition* in mind, see section 2.6.1. For this we have a N-dimensional parallel algorithm that neutralizes a grid. This adds up the values from all the subdomain and makes sure the total of the values is 0.

3.5.3 Dirichlet

Given that we have a slice, representing the dirichlet conditions on the relevant edges, the conditions are easily set by the use of slice-operations. The outermost slice, i.e. ghost layer, is set to be equal to the boundary slice.

3.5.4 Neumann

Chapter 4

Implementation

4.1 General idea

An iterative solver solves a problem by starting with an initial guess, then it performs an algorithm improving the guess and repeats with the improved guess. The difference between the guess and the correct solution, the residual, does not necessarily converge equally fast for different frequencies. An iterative solver can be very efficient on reducing the local error, while the errors due to distant influence is reduced slowly. A multigrid solver attacks this problem by applying iterative methods on different discretizations of the problem, by solving on a very coarse grids the error due to distant influence will be reduced faster, while solving on a fine grid reduces the local error fast. So by solving on both fine and coarse grids the needed cycles will be reduced. To implement a multigrid algorithm we then need algorithms to solve the problem on a grid section 2.5.2, restriction section 2.5.3 and prolongation section 2.5.4 operators to transfer the problem between grids, as well as a method to compute the residual.

4.1.1 V-cycle

The simplest multigrid cycle is called a V-cycle, which starts at the finest grid, goes down to the coarsest grid and then goes back up to the finest grid. First the problem is smoothed on the finest level, then we compute the residual, or the rest after inserting the guess solution in the equation. The residual is then used as the source term for the next level, and we restrict it down as the source term for the next coarser level and repeat until we reach the coarsest level. When we reach the coarsest level the problem is solved there and we obtain a correction term. The correction term is prolongated to the next finer level and added to the solution there, improving the solution, following by a new smoothing to obtain a new correction. This continues until we reach the finest level again and a multigrid cycle is completed, see fig. 2.3 for a 3 level schematic.

In the following description of the steps in the MG method, we will use ϕ , ρ , d and ω to signify the solution, source, defect and correction respectively. A subscript means the grid level, where 0 si the finest level, while the superscript 0 implies an initial guess is used. Hats and tildes are also used to signify the stage the solution is in, with a hat meaning the solution is smoothed and a tilde meaning the correction from the grid below is added.

The overarching algorithm is shown in algorithm 2

Algorithm 2 Multigrid V cycle

```

if level = coarsest then
    Solve           |  $\hat{\phi}_l = \mathcal{S}(\phi_l, \rho_l)$ 
    Interpolate correction |  $\omega_{l-1} = \mathcal{I}\phi_l$ 
else
    for each level do
        Smooth           |  $\hat{\phi}_l = \mathcal{S}(\phi_l, \rho_l)$ 
        Residual          |  $d_l = \nabla^2\hat{\phi}_l - \rho_l$ 
        Restrict           |  $\rho_{l+1} = \mathcal{R}d_l$ 
        Go down, recieve correction |  $\omega_l = \text{MG}(\phi_{l+1})$ 
        Add correction    |  $\tilde{\phi}_l = \hat{\phi}_l + \omega_l$ 
        Smooth           |  $\phi_l = \mathcal{S}(\tilde{\phi}_l, \rho_l)$ 
        Interpolate correction |  $\omega_{l-1} = \mathcal{I}\phi_l$ 

```

At the coarsest level the the problem is solved directly and the correction is propageted upward.

4.1.2 Updating the Halo

All of the subgrids has a halo of ghostslayers around it, which is used to simplify boundary conditions and subdomain communication. Each computational node represents a subdomain of the whole, with the neighboring node being the boundary. So between two subdomains each subdomain updates the boundary according to the neigbouring subdomain. In addition the halo is used to facilitate boundary conditions on the whole domain. For some of the grid operators the ghost are not used, while some of them need updated values. All of the iterative solvers, that are used for smoothing, need updated values of the of the solution, ϕ . The prolongation and residual operators need updated values for the solution ϕ , and the restrictor need updated residual values, ρ , as long as direct insertion is not used. (NOTE TO SELF: belong in paralellization part) We also need to take into account that the smoothers outputs an updated halo for ϕ , to avoid unnecessarily communication between the processors.

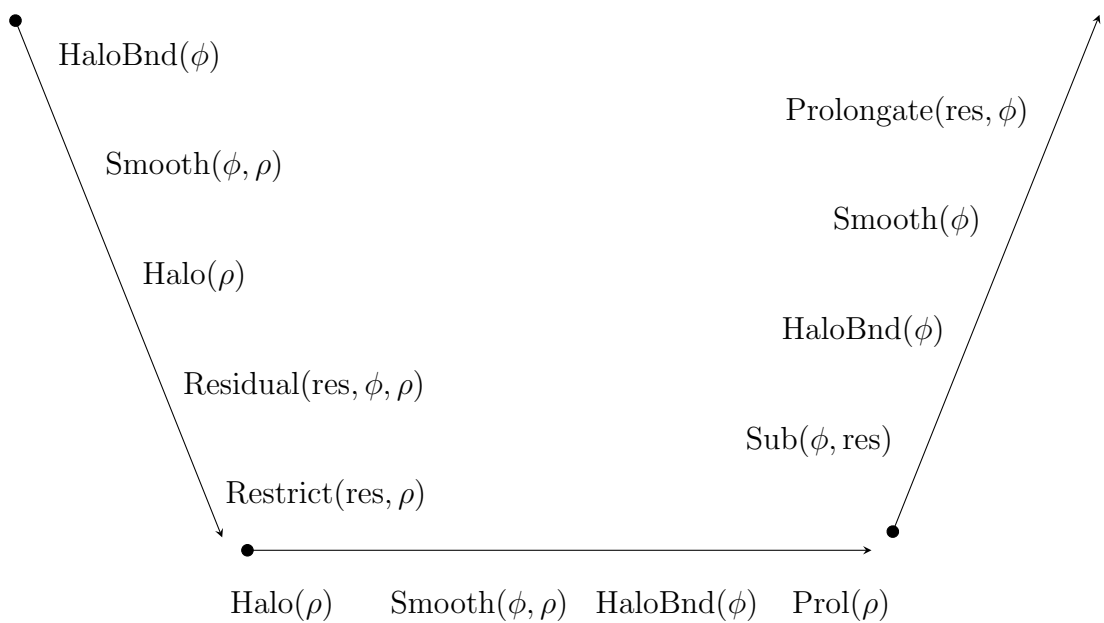


Figure 4.1: The functions used in 2 grid deep multigrid. The algorithm follows the

4.1.3 Implementation

In general there are 4 different quantities, the source, the solution, the residual and the correction, we need to keep track of. On each grid level the residual is computed, then it is set as the source term for the next level and then it is not used more. The correction, the improvement to the finer grid, is only used when going to a finer grid. Due to this we can save some memory by letting the correction and the residual share the same memory, so both are stored in the mgRes struct. There are a regular as well as a recursive implementation of a V-cycle. The functions takes the current level, the bottom of the cycle as well as the end point of the cycle. So several different cycles can be built from the functions. A W cycle can be built a V cycle that starts at the finest level and stops at a mid level, and then a new V-cycle is started at the mid level that ends at the finest level. A full multigrid algorithm (FMG) can also be implemented by first restricting the original source term down to the coarsest level and then run a V-cycle that ends at the finest level. (Note: there will be a a general mgSolver function pointer that can be set to prebuilt cycles, so the cycle can be set from the input file)

The regular V cycle algorithm is quite straightforward, first it restricts and computes itself down to the bottom level, then it solves it directly on the bottom level. Then the correction is brought up and improved through the grid up to the top level. See ?? for an example code.

The recursive algorithm uses an algorithm more similar to the one described in ?. First it computes the steps necessary so the grid below has an updated source term, then it calls itself on a lower level. After receiving the correction from the lower level it is improved and sent to the level above. If the function is at the bottom level, it solves the problem directly and sends the correction up. See ?? for an example code.

4.2 Restriction

In our implementation we first cycle through all of the true coarse grid points, then the two main tasks is to find the specific fine grid point corresponding to the specific coarse grid point, and finding the indexes of the fine grid points surrounding the grid point.

Since the value in both grids are stored in a first order lexicographical array, we should treat the grid points in the same fashion, so the values are stored close to each other in the array. The first dimension is treated first, then the next is dimension is incremented followed by treating the first dimension again, then increment the next and so on. The fine grid has twice the resolution of the coarse grid, so for each time the coarse grid index is incremented, the fine grid index is incremented twice.

Along the x-axis each incrementation is the number of values stored in the grid, which for scalars is 1 (This is only used for scalars, so now the 1 is hardcoded, I will need to test if using `size[0]` instead affects speed), and 2 for the fine index. The fine index will in addition need to skip 1 row each time, each time the y-axis is incremented, due to the finer resolution and 1 layer each time the z-axis is incremented.

At the edges of the grid we have ghost layers, which have equal thickness for both the grids, so the coarse grid needs to increment over the ghost values, in the x-direction, each time y is incremented. When z is incremented the index need to skip over a row of ghost values. The fine index follows the same procedure as the coarse index when dealing with the ghost layers.

When correct fine grid index is found, corresponding to a coarse grid index, the stencil needs to be applied around that grid value. This is done by first calculating the index of the first coarse and find indexes and setting the correct indexes for the surrounding grid values, then the surrounding grid indexes can be incremented exactly as the fine grid index and they will keep their shape around the fine grid index. Since our indexes in x, y and z are labeled j,l,k, the next value along the x-axis is labeled 'fj' and the previous is labeled 'fjj'. The coarse and fine grid indexes are label 'c' and 'f' respectively.

4.3 Prolongation

The algorithm implemented for the interpolation is based on the method, described in Press et al., 1988, has the following steps, which is also shown for a 2D case in 4.2.

1. Direct insertion: Coarse→ Fine
2. Interpolation on highest Dimension: $f(x) = \frac{f(x+h)+f(x-h)}{2h}$
3. Fill needed ghosts.
4. Interpolation on next highest Dimension

The interpolation should always first be done on the highest dimension, because the grid values are stored further apart along the highest axis in the memory, and the each successive interpolation needs to apply to more grid points. (Note to self: should test)

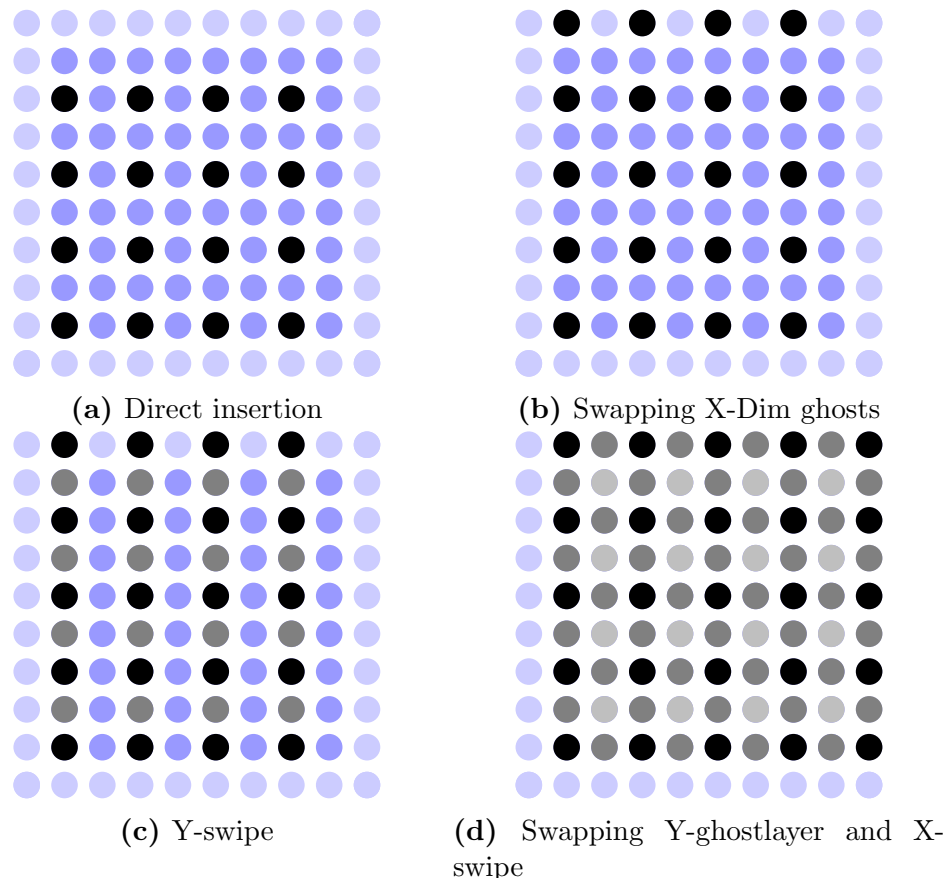


Figure 4.2: This figure shows the steps in computing the prolongation stencil in an $[8 \times 8]$ grid. First a direct insertion from the coarse grid is performed (4.2a), followed by filling the ghostlayer perpendicular to the x-axis from the neighbouring grid (4.2b). Then a swipe is performed in the y-direction filling the grid points between, taking half the value from the node above, and half from the node below (4.2c). Then a ghost swap is performed before doing a swap in the x-direction (4.2d).

4.4 Smoothers

Jacobi's method

The implementation of the jacobian algorithm is straightforward, but it has the downside of slow convergence and bad smoothing properties, in addition to needing an additional grid values. When ϕ_i^{n+1} is computed we need access to the previous value ϕ_{i-1}^n , and more values in higher dimensions, so either the previous values need to stored seperately, or ϕ_i^{n+1} can be computed on a new grid and then copied over after completing the cycle. In this implementation we computed on a temporary grid and then copied over, since it was mostly for debugging purposes and efficiency was not a concern.

The computation is done by starting at index $g = 0$, computing the surrounding grid indexes, gj, gjj, \dots , where gj is the next grid point along the x-axis, and gjj is the previous value. Then the entire grid is looped trough over, incrementing both g and the surrounding grid indexes gj, gjj, \dots . The computation on the ghost layers will be incorrect but those will be overwritten when swapping halos. See ?? for an example code in 2D.

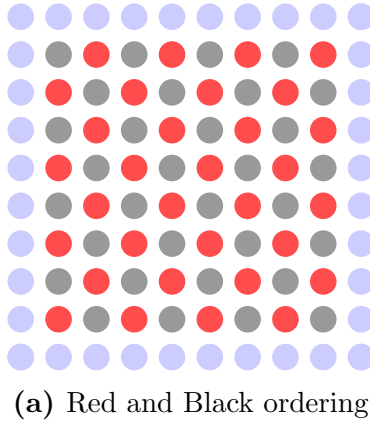
Gauss-Seidel Red and Black

In the implementation of Gauss-Seidel algorithm we use a clever ordering of the computations, called Red and Black ordering, both to increase the smoothing properties of the algorithm as well as avoiding creating a temporary grid to store ϕ^{n+1} in. Every grid point where the indexes sum up to an even number is labeled a red point and the odd index groupings are labeled black points, see fig. 4.3a. Then each red point is directly surrounded by only black points and vica versa.

A cycle is then divided into 2 halfcycles, where each halfcycle computes ϕ^{n+1} for the red and black points respectively.

1. for(int c = 0; c<nCycles; c++)
 - Cycle through red points and compute ϕ^{n+1}
 - Swap Halo
 - Cycle through black points and compute ϕ^{n+1}
 - Swap Halo

For the 2 dimensional case the cycling is done first for the odd rows and even rows seperately, due to the similarity between all the red points in the odd rows, and between the red points in the even rows. Then the cycling could be generalized into a static inline function used for all the cycling. See ?? for the 2D implementation.



(a) Red and Black ordering

For the 3 dimensional case there is now did two different takes on the problem, one where the iteration through the grid is streamlined, but needing several loops through the grid taking care of a subgroup of the grid points each loop. The other algorithm uses one loop through the grid, with different conditions on the edges to make it go through the correct grid points in each line.

When the loops are streamlined the edges the loop go through the entire grid, but when it reaches and edge in it either needs to add or subtract 1 to the iterator index. In we want to do a red pass, computing all the red values, the grid is cycled through increasing by 2 each time. Then it will access up the indexes, 36, 38, 40, 42, … . In the second row we want it to use the index 43, instead of 42, so we need to increase it by 1 when it reaches the edge. When it reaches the end of the second line, we want it to increase from 47 to 48, so then we need to subtract 1. In the next layer we need to shift the behaviour on the edges to the opposite. See

.
48	49	49	50	51	52
42	43	44	45	46	47
36	37	38	39	40	41

In the other implementation I tried something similar to the 2D implementation, where it does several loops through the grid, computing an easier subgroup of the red nodes each time, so the iteration index can increase by just to each time. So for the red points it computes the odd and even layers and rows seperately.

- Compute Odd layers, odd rows
- Compute Odd layers, even rows
- Compute Even Layers, odd rows
- Compute Even layers, even rows

4.5 Implementation of Boundary Conditions

Since the subdomains already need to exchange the halo, we already had made a suite of function dealing with halo-operations. These functions can get, set, add, etc. N-dimensional slices from the halo. As can be seen in ?? this is quite similar to the needs of the varying boundary conditions and we will reuse this capability during the implementation of boundary conditions. In addition we will also need methods to restrict the part of the conditions that need to be restricted. Here we will only deal with time-invariant boundary conditions so they can be set, and restricted, once during initializations of the grids. It should be easy to expand it to time varying conditions, just restrict the boundary function each timestep.

In general the condition types are stored as a 2Dim array, in the order $x_{low}, x_{upper}, y_{low}, \dots$. Each time the boundary conditions function is called it checks if each subdomain edge is at the total domain boundary. Since the outer subdomains need to do extra computations here, it shouldn't matter if the inner subdomains do some extra calculations. If the subdomain boundary is at the boundary it calls the a function depending on which boundary type the edge is.

4.5.1 Restriction

For now we have choosen to use straight injection, since we will not use any complicated boundary conditions in this project, other developers are welcome to expand it by more restriction algorithms.

4.5.2 Periodic

The periodic boundary conditions are just the same procedure as the halo exchange. To try too keep an even load, between the computational nodes, the halo exchange is also done between the the boundary subdomains.

To keep the convergence rate good we also need to keep the *global constraint* and *compatibility condition* in mind, see section 2.6.1. For this we have a N-dimensional parallel algorithm that neutralizes a grid. This adds up the values from all the subdomain and makes sure the total of the values is 0.

4.5.3 Dirichlet

Given that we have a slice, representing the dirichlet conditions on the relevant edges, the conditions are easily set by the use of slice-operations. The outermost slice, i.e. ghost layer, is set to be equal to the boundary slice.

4.5.4 Neumann

Chapter 5

Verification

In this chapter we will go through different methods we used to verify the multi-grid solver, as well as scaling measurements. Modular parts of the solver is tested with unittests where feasible. In addition the whole solver is tested with both analytically solvable test cases and randomly generated fields.

5.0.1 Error Quantification

In order to evaluate solutions we will primarily look at the normalized 2-norm of the error, eq. (5.1), and the residual, eq. (5.2). The $\|e\|_2$ is computed from comparing the numerical solution $\hat{\phi}$ to an analytical solution ϕ and normalized with regards to grid points, N . The residual is found by inserting the numerical solution into the Poisson equation, the remaining part is then the residual, and shows the difference of the current numerical solution and the optimal numerical solution.

$$\|e\|_2 = \sqrt{\frac{\sum (\hat{\phi} - \phi)^2}{N}} \quad (5.1)$$

$$\bar{r} = \frac{1}{N} \left(\sum_i \nabla^2 \hat{\phi}_i + \rho_i \right) \quad (5.2)$$

5.1 Multigrid Solver

To test the solver itself we employ a couple different techniques. First we create a charge distribution by differentiating a known potential, and then running the solver and check the difference to the original potential.

For the second test we use a charge distribution with a known analytical solution, and we then we compare the numerical solution to the analytical solution.

Since constructed solutions can often behave to nice, we will also perform a third test on a randomized charge distribution, here we will only look at the residual since we cannot compute the error due to not having an analytical solution. We expect the residual to approach 0.

Lastly we perform a few run on identical charge distributions, domain subdivisions and compare the solutions.

5.1.1 Analytical Solutions

We use a few different constructed charge density fields, which is analytically solvable, to test the performance and correctness of the solver. All the simulations here are ran on a grid of the size 128, 64, 64 divided into 1, 2, 2 subdomains, with pinc version 36ad. It uses 5 cycles when presmoothing, solving on the coarsest grid and postsmothing, the MG solver is instructed to run for 100 MG V-cycles with 2 grid levels.

Sinusoidal function

A sinusoidal source term, ρ can be useful to test the solver since it can be constructed to have very simple derivatives and integrals. Here we use a sinusoidal function that has two positive tops and two negative tops over the total domain. We want the sinus function to go over 1 period over the domain, so we normalize the argument by dividing the grid point value, x_j, y_k, z_l , by the domain length in the direction, L_x, L_y, L_z .

$$\rho(x_j, y_j, z_l) = \sin\left(x_j \frac{2\pi}{L_x}\right) \sin\left(y_k \frac{2\pi}{L_y}\right) \quad (5.3)$$

A potential that fits with this is:

$$\phi(x, y, z) = -\left(\frac{2\pi}{L_x}\right)^2 \left(\frac{2\pi}{L_y}\right)^2 \sin\left(x_j \frac{2\pi}{L_x}\right) \sin\left(y_k \frac{2\pi}{L_y}\right) \quad (5.4)$$

The fig. 5.1 shows the results from running the MG-solver on the test sinusoidal test case described here. As can be expected the potential mirrors the charge distribution, except with an opposite sign and a larger amplitude. A decently large grid was simulated and the mean residual was found to be: $\bar{r} \approx 0.0312$.

Heaviside Function

The solver is also tested with a charge distribution governed by a Heaviside function. This is also suited to testing since the charge distribution is then

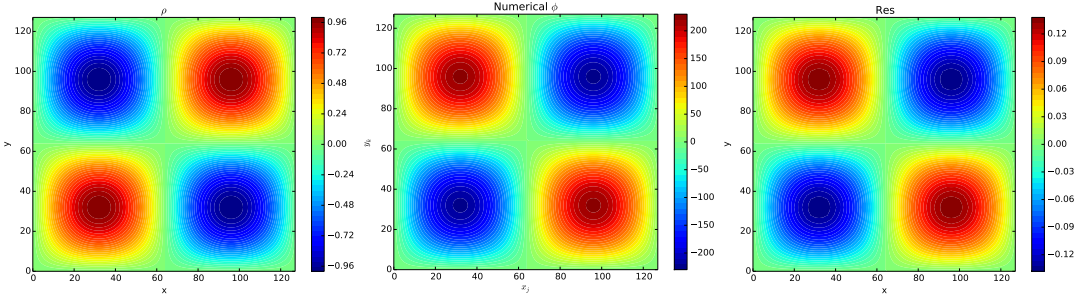


Figure 5.1: This a x, y -plane from the grids cut along $z_l = 32$, from the sinusoidal test case described in section 5.1.1. The left plot shows the charge distribution, the center plot shows the numerical solution of the potential and the plot to the right depicts the residual.

constant planes, and we expect second order polynomial when integrating them. In the test case there are two planes with the value -1 and two planes with 1 . In fig. 5.2 the test case, as well as the solution and residual is shown, and we can see the polynomials in the solution. The mean residual \bar{r} was 0.00677 .

$$\rho(x_j, y_k, z_l) = \begin{cases} 1 & y_j \epsilon(0, 32), (64, 96) \\ -1 & y_j \epsilon(33, 65), (97, 127) \end{cases} \quad (5.5)$$

5.1.2 Random Charge distribution

To hopefully avoid some problems, that could appear due to the earlier test cases being to constructed being to orderly, a test with a randomized charge distribution is also included. The fig. 5.3 shows the charge distribution, numerical potential and the residual. The mean residual was found to be $\bar{r} \approx 0.00388$.

5.2 Scaling of the error compared to discretization

The solver is solving a discretized problem, due to this the solution will not be exact. The error will be of second order, $\mathcal{O}(h^{-2})$, dependent on the stepsize, h , due to the first order solver, see section 2.5.2.

To investigate that the error the of the solver follows a second order improvement as the stepsize decreases we construct a sinusoidal rho as a test case.

$$\rho(x) = \sin\left(\frac{x}{2\pi}\right) \quad ; \quad x \in [0, 2\pi] \quad (5.6)$$

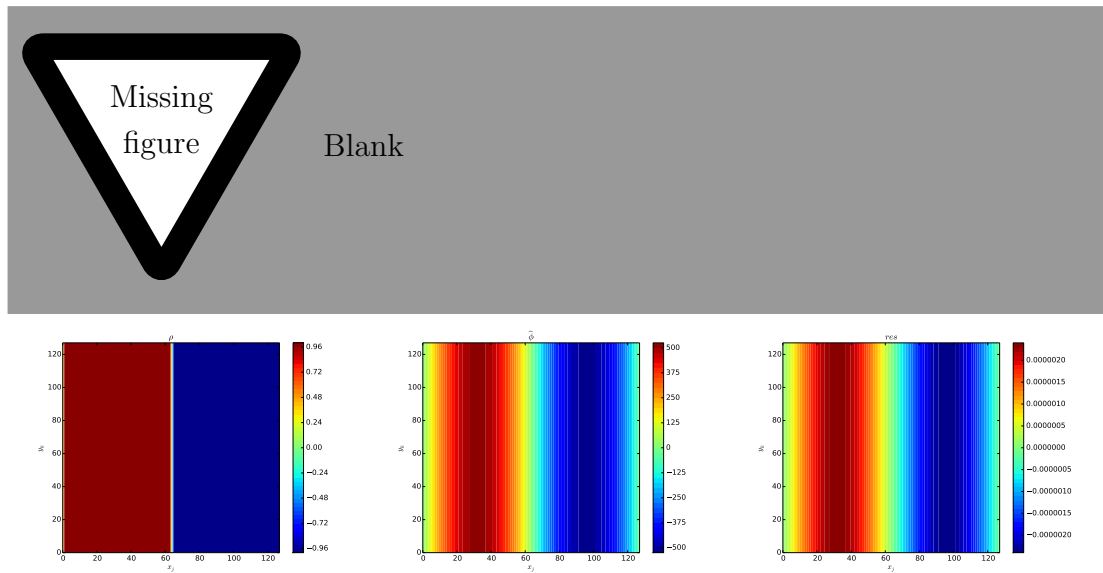


Figure 5.2: As earlier this is a x, y -plane cut along $x_k = 32$, of the grid. The plots show the charge distribution, numerical solution and the solution, from left to right. This is a test case constructed with Heaviside functions. In the solution of the potential the expected second degree polynomial can be seen.

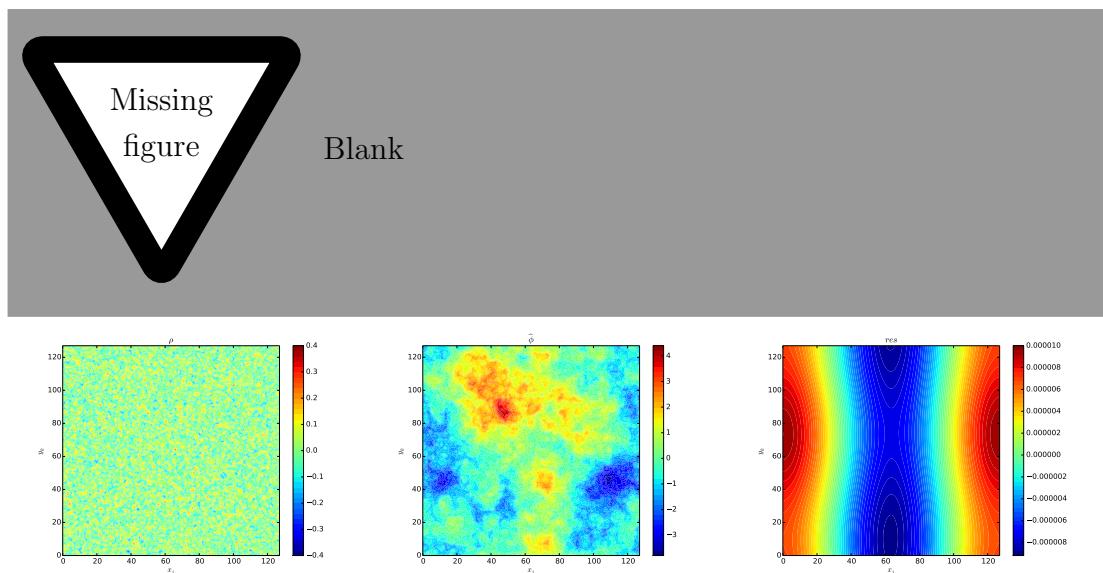


Figure 5.3: As earlier this is a x, y -plane cut along $x_k = 32$, of the grid. The plots show the charge distribution, numerical solution and the solution, from left to right.

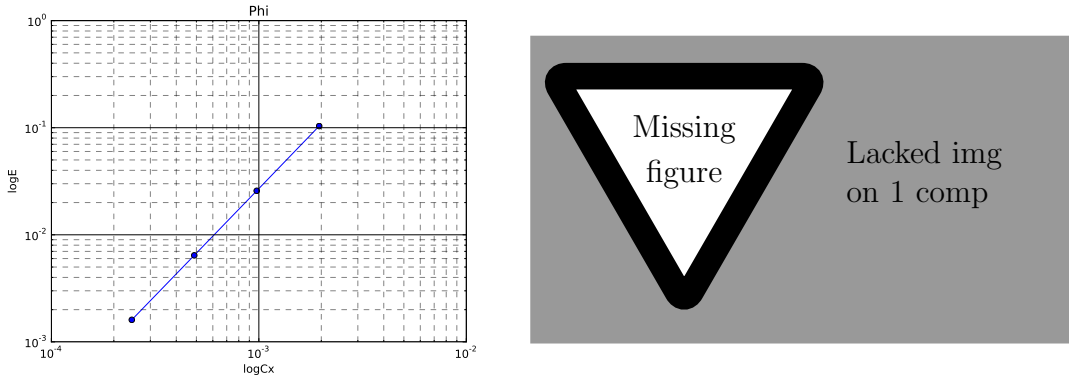


Figure 5.4: Logarithmic plot of the 2-norm of the error of the potential ϕ , left figure, and the x-component of the electric field. The solver was run on a scaled sinus-shaped charge distribution. Both of the plots show a straight line of the error, on the logarithmic plots, with a slope of 2.00. This correspond to maximal error of $\mathcal{O}(h^2)$

This ρ is analytically solvable for the Poisson equation so we can compute the 2-norm of the error, $\|err\|_2$. Then we gradually decrease the stepsize and obtain and compare the norm of the numerical solutions. Since the normalization in PinC is normally done outside the multigrid solver, rho had to be suitably scaled to the stepsize. We expect the error proportional to the squared stepsize, $err(h) \approx Ch^2$, so by taking the logarithm we obtain

$$\log(err(h)) = 2 \log(Ch) \quad (5.7)$$

where C is a constant dependent on ρ . fig. 5.4 shows the the measured error when solving the sinusoidal charge distribution, eq. (5.6), for both the potential, ϕ , and the electric field, E_x . The problem was solved with different discretizations on a 3-dimensional domain, starting at [8, 8, 8] doubling the grid points each time. The slope on the logarithmic plots was in both cases found to be 2.00, showing a second order error $\mathcal{O}(h^{-2})$. The same test was also performed in 1 and 2 dimensional cases, with varying subdomain configurations and with the sinus shape along the other axes.

5.2.1 Langmuir Oscillation Test Case

As a test of the validity of our PiC program, we can use the langmuir wave oscillation. This test is inspired by a case set up in Birdsall and Langdon (2004), and modified to fit with our normalization and discretizations.

5.3 Plasma Oscillation

- Plasma oscillates
- Randomly distributed plasma, with random velocities (Vel Causing a bug-
↳ Fix)
- Compute fitting Temperature and Debye length

5.3.1 Input parameters

Timestep

First we need to ensure that the simulation is does not violate the time- stability criterion, section 2.2.1, $\Delta t \leq 2\omega_{pe}$. For computational reasons each particle in the program represents many real particles and we can adjust the number, of real particles represented, to ensure that the electron plasma frequency is 1.

$$\omega_{pe}^2 = \frac{nq_e^2}{m\epsilon_0} = \left(\frac{N}{V}\right) \left(\frac{q_{e*}}{m_{e*}}\right) q_{e*} \quad (5.8)$$

Here (N/V) is just the number of electron super-particles divided by the volume, q_e and m_e , represents super-particles and needs to be multiplied by the number of particles in a super-particle, κ .

$$\omega_{pe}^2 = \left(\frac{N}{V}\right) \left(\frac{e}{m_e}\right) \kappa e \quad (5.9)$$

Since we want the electron plasma frequency to be 1, κ is set to

$$\kappa = \frac{Vm_e}{Ne^2} \quad (5.10)$$

Now the time is given in units of ω_{pe} and we use $\Delta t = 0.2 < 2$ easily.

Spatial-step

The spatial step need to satisfy the finite grid instability condition, $\Delta x < \zeta \lambda_{Se}$, section 2.2.3. We use a similar procedure as in normalizing the time with regards to ω_{pe} to normalize the length with regards to λ_{Se} . Then we end up with the temperature, or its other representation as thermal velocity, as the parameter we can adjust to make sure that it satisfies the condition.

$$\lambda_{Se}^2 = \frac{\epsilon_0 k T_e}{n q_e^2} \quad (5.11)$$

Chapter 6

Performance/Results

6.1 Scaling

In this section we investigate the performance of the solver and different scaling measurements. We are interested in both how well the solver performs on a larger number of processors, as well as the performance impact of the different parameters in the solver.

We want to obtain a better understanding of how the field resolution can be scaled up without hampering the performance of the particle-in-cell simulation too much.

6.1.1 Performance Optimizer

A multigrid solver has several parameters that need to be set correctly for optimal performance (Find Source for!!!). These parameters are dependent on the problem size, as well as the computing architecture. Instead of attempting to estimate them beforehand we have included an external script that runs the program with different MG-solver settings on the wanted domainsize and tries to optimize them. The parameters it tries to change is the number of grid levels and the cycles to run for presmoothing, postsMOOTHing and the coarse solver. It should be worth it to spend some computing power, finding close to optimal settings, prior to running a full scale simulation since the solver needs to run each time step. The performance optimizer naively runs the solver for a predetermined mesh of settings.

1. Smarter testing algorithm 'if better when increase continue increasing, else stop'

NOTE TO SELF: This didn't pan out very well

6.2 Processor scaling

Now we want to investigate how well the solver is parallelized. In section 2.7.6 the theoretical considerations for how it should scale is gone through.

6.2.1 Convergence Rate

As an iterative solver a multigrid solver will gradually approach a solution, reducing the residual further each run. In this subsection we will measure the convergence rate, defined in similar way as in Zhukov et al. (2014),

$$p = \left(\frac{r_m}{r_0} \right)^{1/m} \quad (6.1)$$

where r_m, r_0 are the 2-norm of a the residual after m multigrid runs and the initial residual. We presume that each run of the multigrid solver will remove a proportion of the remaining residual. The tests are done on a 128^3 grid on a sinusoidal problem, and the smoothers run for an equal number of runs on each level. (Table of convergence rate numbers) Zhukov et al. found convergence rates of $p \approx 0.15$ and $p \approx 0.17$ using a multigrid solver with a Chebyshev algorithm to smooth.

6.2.2 Scaling of the MG Solver

One of the aims of building a parallel multigrid solver was to be able to enable simulating large plasma problems. To be able to achieve that the solver should be able to scale up very well, i.e. doubling the problem size and the number of available processors should only give a manageable increase in computational time. We don't expect to be able to achieve a perfect parallelization, since there is a certain amount of interprocessor communications necessary that will slow down the algorithm compared to a sequential algorithm. The exact parallel performance is also dependent on the communications channels and the topology between the processor clusters. In section 2.7.6 the parallel complexities for the different multigrid algorithms is given and we will look at the parallel properties for a V, W and FMG algorithm.

To investigate the scaling properties we will run set up a standard problem, and solve it with increasing resolutions. We start with a 64^3 grid on 1^3 computaional core, then we increase the problemsize to 128^3 on 2^3 and so on. These tests were run on (FIND ABEL SPECS). (PUT IN FIGURE OF SCALING (Processors/Time))

6.2.3 Scaling properties PiC

As well as the scaling properties of the multigrid solver a look at the whole PiC model is interesting. This helps us easier pinpoint where further optimizations efforts should be directed. We do not necessarily expect the the particle based algorithms to scale up to larger problems in the same rate as the solver. So above a certain number of processors, or size, there may be a bottleneck.

Bibliography

- Adams, M. F. (2001). “A distributed memory unstructured Gauss-Seidel algorithm for multigrid smoothers”. In: Supercomputing, ACM/IEEE 2001 Conference. IEEE, pp. 14–14. URL: http://ieeexplore.ieee.org/xpls/abs_all.jsp?arnumber=1592790 (visited on 04/21/2016).
- Alnæs, M. S. et al. (2011). The FEniCS Manual. October. URL: <http://mmc2.geofisica.unam.mx/acl/edp/Ejemplitos/FEniCs/fenics-manual-2011-10-31.pdf> (visited on 04/21/2016).
- Arraras, A. et al. (2015). “Domain decomposition multigrid methods for nonlinear reaction–diffusion problems”. In: Communications in Nonlinear Science and Numerical Simulation 20.3, pp. 699–710. URL: <http://www.sciencedirect.com/science/article/pii/S1007570414003074> (visited on 04/21/2016).
- Baumjohann, W. and R. A. Treumann (1997). Basic Space Plasma Physics. en. Google-Books-ID: e4yupcOzJxkC. World Scientific. ISBN: 978-1-86094-079-8.
- Bertrand, P. et al. (1990). “A nonperiodic Euler–Vlasov code for the numerical simulation of laser–plasma beat wave acceleration and Raman scattering”. In: Physics of Fluids B: Plasma Physics (1989-1993) 2.5, pp. 1028–1037. ISSN: 0899-8221. DOI: [10.1063/1.859276](https://doi.org/10.1063/1.859276). URL: <http://scitation.aip.org/content/aip/journal/pofb/2/5/10.1063/1.859276> (visited on 08/24/2016).
- Birdsall, C. K. and A. B. Langdon (2004). Plasma Physics via Computer Simulation. en. CRC Press. ISBN: 978-1-4822-6306-0.
- Buneman, O. (1959). “Dissipation of Currents in Ionized Media”. In: Physical Review 115.3, pp. 503–517. DOI: [10.1103/PhysRev.115.503](https://doi.org/10.1103/PhysRev.115.503). URL: <http://link.aps.org/doi/10.1103/PhysRev.115.503> (visited on 08/19/2016).
- Chen, F. F. (1984). Introduction to Plasma Physics and Controlled Fusion. en. Boston, MA: Springer US. ISBN: 978-1-4419-3201-3 978-1-4757-5595-4. URL: <http://link.springer.com/10.1007/978-1-4757-5595-4> (visited on 07/12/2016).
- Chow, E. et al. (2006). “A survey of parallelization techniques for multigrid solvers”. In: Parallel processing for scientific computing 20, pp. 179–201. URL: <http://www.edmondchow.com/pubs/parmg-survey-siam.pdf> (visited on 04/21/2016).
- Courant, R. et al. (1869). “Über die partiellen Differenzengleichungen der mathematischen Physik - PPN235181684_0100__log5.pdf”. In: Mathematische Annalen

100. URL: http://www.digizeitschriften.de/download/PPN235181684_0100/PPN235181684_0100__log5.pdf (visited on 09/27/2016).
- Cummings, W. D. and A. J. Dessler (1967). “Field-aligned currents in the magnetosphere”. en. In: Journal of Geophysical Research 72.3, pp. 1007–1013. ISSN: 2156-2202. DOI: [10.1029/JZ072i003p01007](https://doi.org/10.1029/JZ072i003p01007). URL: <http://onlinelibrary.wiley.com/doi/10.1029/JZ072i003p01007/abstract> (visited on 07/19/2016).
- Dawson, J. (1962). “One-Dimensional Plasma Model”. In: Physics of Fluids (1958-1988) 5.4, pp. 445–459. ISSN: 0031-9171. DOI: [10.1063/1.1706638](https://doi.org/10.1063/1.1706638). URL: <http://scitation.aip.org/content/aip/journal/pof1/5/4/10.1063/1.1706638> (visited on 08/19/2016).
- Fitzpatrick, R. (2014). Plasma Physics: An Introduction. English. 1 edition. Boca Raton: CRC Press. ISBN: 978-1-4665-9426-5.
- Friedman, A. et al. (1981). “A direct method for implicit particle-in-cell simulation”. In: Comments on Plasma Physics and Controlled Fusion 6.6, pp. 225–236. ISSN: ISSN 0374-2806. URL: http://inis.iaea.org/Search/search.aspx?orig_q=RN:15000463 (visited on 11/06/2016).
- Goldston, R. J. and P. H. Rutherford (1995). Introduction to Plasma Physics. en. CRC Press. ISBN: 978-1-4398-2207-4.
- Hackbusch, W. and U. Trottenberg (1982). “Multigrid methods”. In: URL: <http://158.69.150.236:1080/jspui/handle/961944/66389> (visited on 04/21/2016).
- Hawley, J. F. and J. M. Stone (1995). “Numerical Methods in Astrophysical HydrodynamicsMOCCT: A numerical technique for astrophysical MHD”. In: Computer Physics Communications 89.1, pp. 127–148. ISSN: 0010-4655. DOI: [10.1016/0010-4655\(95\)00190-Q](https://doi.org/10.1016/0010-4655(95)00190-Q). URL: <http://www.sciencedirect.com/science/article/pii/001046559500190Q> (visited on 08/24/2016).
- Hjorth-Jensen, M. (2016). Computational Physics - Lecture Notes Fall 2013. URL: <http://www.physics.ohio-state.edu/~ntg/6810/readings/Hjorth-Jensen-lectures2013.pdf> (visited on 08/22/2016).
- Hockney, R. W. and J. W. Eastwood (1988). Computer Simulation Using Particles. en. Google-Books-ID: nTOFkmnCQuIC. CRC Press. ISBN: 978-1-4398-2205-0.
- Israeli, M. and A. Sherman (2005). “An Accurate Fourier-spectral Solver for Variable Coefficient Elliptic Equations”. In: Proceedings of the 5th WSEAS/IASME International ISTASC'05. Stevens Point, Wisconsin, USA: World Scientific, Engineering Academy, and Society (WSEAS), pp. 152–156. ISBN: 978-960-8457-35-5. URL: <http://dl.acm.org/citation.cfm?id=1373616.1373642> (visited on 11/06/2016).
- Lapenta, G. (2016). Particle In Cell Methods. With Application to Simulations in Space. Weather URL: <https://perswww.kuleuven.be/~u0052182/pic/book.pdf> (visited on 09/27/2016).
- Pécseli, H. L. (2012). Waves and Oscillations in Plasmas. English. 1 edition. Boca Raton: CRC Press. ISBN: 978-1-4398-7848-4.

- Press, W. H. et al. (1988). “Numerical recipes in C”. In: Cambridge University Press 1, p. 3. URL: http://journals.cambridge.org/abstract_S0269964800000565 (visited on 04/21/2016).
- Qin, H. et al. (2013). “Why is Boris algorithm so good?” In: Physics of Plasmas (1994-present) 20.8, p. 084503. ISSN: 1070-664X, 1089-7674. DOI: [10.1063/1.4818428](https://doi.org/10.1063/1.4818428). URL: <http://scitation.aip.org/content/aip/journal/pop/20/8/10.1063/1.4818428> (visited on 11/06/2016).
- Sgattoni, A. et al. (2015). piccante: arXiv:1503.02464. DOI: [10.5281/zenodo.16097](https://doi.org/10.5281/zenodo.16097). URL: <http://zenodo.org/record/16097> (visited on 08/22/2016).
- Shen, J. (1994). “Efficient Spectral-Galerkin Method I. Direct Solvers of Second- and Fourth-Order Equations Using Legendre Polynomials”. In: SIAM Journal on Scientific Computing 15.6, pp. 1489–1505. ISSN: 1064-8275. DOI: [10.1137/0915089](https://doi.org/10.1137/0915089). URL: <http://pubs.siam.org/doi/abs/10.1137/0915089> (visited on 04/21/2016).
- Shu, F. H. (2010). The Physics of Astrophysics Volume I: Radiation. English. Mill Valley, Calif.: University Science Books. ISBN: 978-1-891389-76-4.
- Stüben, K. (2001). “A review of algebraic multigrid”. In: Journal of Computational and Applied Mathematics 128.1, pp. 281–309. URL: <http://www.sciencedirect.com/science/article/pii/S0377042700005161> (visited on 04/21/2016).
- Swendsen, R. H. (2006). “Statistical mechanics of colloids and Boltzmann’s definition of the entropy”. In: American Journal of Physics 74.3, pp. 187–190. ISSN: 0002-9505, 1943-2909. DOI: [10.1119/1.2174962](https://doi.org/10.1119/1.2174962). URL: <http://scitation.aip.org/content/aapt/journal/ajp/74/3/10.1119/1.2174962> (visited on 07/22/2016).
- Trottenberg, U. et al. (2000). Multigrid. Academic press. URL: <https://www.google.com/books?hl=en&lr=&id=9ysyNPZoR24C&oi=fnd&pg=PP1&dq=trottenberg+2000&ots=rJCHSPzSMY&sig=sin3i-gmWOoykoTFnyHGIPZXT5Q> (visited on 04/21/2016).
- Verboncoeur, J. P. (2005). “Particle simulation of plasmas: review and advances”. en. In: Plasma Physics and Controlled Fusion 47.5A, A231. ISSN: 0741-3335. DOI: [10.1088/0741-3335/47/5A/017](https://doi.org/10.1088/0741-3335/47/5A/017). URL: <http://stacks.iop.org/0741-3335/47/i=5A/a=017> (visited on 07/21/2016).
- Watanabe, K. and T. Sato (1990). “Global simulation of the solar wind-magnetosphere interaction: The importance of its numerical validity”. en. In: Journal of Geophysical Research: Space Physics 95.A1, pp. 75–88. ISSN: 2156-2202. DOI: [10.1029/JA095iA01p00075](https://doi.org/10.1029/JA095iA01p00075). URL: <http://onlinelibrary.wiley.com/doi/10.1029/JA095iA01p00075/abstract> (visited on 08/24/2016).
- Zhukov, V. T. et al. (2014). “Parallel multigrid method for solving elliptic equations”. en. In: Mathematical Models and Computer Simulations 6.4, pp. 425–434. ISSN: 2070-0482, 2070-0490. DOI: [10.1134/S2070048214040103](https://doi.org/10.1134/S2070048214040103). URL: <http://link.springer.com/article/10.1134/S2070048214040103> (visited on 10/17/2016).